1974

# Neutron penetration using the transfer matrix method

Te-Chang Chan
*Iowa State University*

# Neutron penetration using the transfer matrix method

by

Te-Chang Chan

A Dissertation Submitted to the

Graduate Faculty in Partial Fulfillment of

The Requirements for the Degree of

DOCTOR OF PHILOSOPHY

Department: Chemical Engineering and Nuclear Engineering
Major: Nuclear Engineering

Approved:

Signature was redacted for privacy.

In Charge of Major Work

Signature was redacted for privacy.

For the Major Department

Signature was redacted for privacy.

For the Graduate College

Iowa State University
Of Science and Technology
Ames, Iowa

1974

TABLE OF CONTENTS

# LIST OF SYMBOLS

$A$ = $(\alpha + \beta)(\alpha - \beta)$

$A'_k$ = coefficient in the half-range Legendre polynomial for expansion of a Legendre polynomial

$A_{\ell k}$ = $\dfrac{(-1)^k(\ell + k)!}{2^k k!(\ell - k)!}$

$B_{\ell k}$ = coefficient of expansion of the $\ell$th angular distribution due to point source

$B_{\pm}$ = matrices related to the transfer matrix H

$C_{\pm}$ = matrices related to the transfer matrix H

$d^{\ell}_{mn}(\mu_o)$ = $\displaystyle\int_0^1 d\omega \int_0^1 d\omega' P_{\ell}(\omega) P_{\ell}(\omega') P^{+}_{m}(\omega) P^{+}_{n}(\omega')$

$D_{\ell}(\mu_o)$ = matrix of the $d^{\ell}_{mn}(\mu_o)$

$D^{n}_{x}$ = nth partial derivative with respect to x

$D^{-n}_{x}$ = n times integration with x as variable

$e_{mn}$ = $\displaystyle\int_0^1 \omega P^{+}_{m}(\omega) P^{+}_{n}(\omega) d\omega$

$E$ = matrix of the $e_{mn}$

$f_{\ell m}$ = $\displaystyle\int_0^1 P_{\ell}(\omega) P^{+}_{m}(\omega) d\omega$

$H_n$ = transfer matrix of layer n

$H(x)$ = transfer matrix of the slab with thickness x

$I$ = unit matrix

$I(x, V, \omega)$ = radiation at (x, V, $\omega$) per unit V per unit solid angle

$I^{pl}_{\ell}(x, V)$ = radiation of moment $\ell$ at (x, V) per unit V due to plane source

$I_{\ell}^{pt}(x, V)$ = radiation of moment $\ell$ at (x, V) per unit V due to point source

L = highest angular expansion term in matrix calculation

$P_{\ell}(\omega)$ = Lengendre polynomial of moment $\ell$ with argument $\omega$

$P_m^+(\omega)$ = half-range Legendre polynomial of moment m with argument $\omega$

r = spatial variable

$R_n$ = reflection matrix operator of layer n

R(x) = reflection matrix operator of the slab with thickness x

$R_{\infty}(x)$ = asymptotic expression of R(x)

S = model matrix of the matrix W

$\underline{S}$ = isotropic radiation source matrix

$T_n$ = transmission matrix operator of layer n

T(x) = transmission matrix operator of the slab with thickness x

$T_{\infty}(x)$ = asymptotic expression of T(x)

V = lethargy after collision

V' = lethargy before collision

$V_g$ = lethargy of group g

W = 2 x 2 matrix of operators containing $\alpha$ and $\beta$

$\overline{W}$ = matrix W after diagonalization

x = slab thickness

$$z_{mn} = \int_0^1 d\omega \int_0^1 d\omega' \delta(\omega - \omega') P_m^+(\omega) P_n^+(\omega')$$

Z = matrix of the $z_{mn}$

$\alpha$ = operator related to the cross sections

$\alpha_{gg'}$ = operator related to the cross sections from group g' to group g

$\beta$ = operator related to the cross sections

$\beta_{gg'}$ = operator related to the cross sections from group g' to group g

$\mu_o$ = cosine of the scattering angle

$\zeta'$ = change of azimuth on scattering

$\omega$ = cosine of angle between direction of radiation and normal to slab

$\Omega$ = unit vector in direction of particle velocity after scattering

$\Omega'$ = unit vector in direction of particle velocity before scattering

$\Lambda$ = eigenvalue matrix of the transfer matrix H

$\sigma_t(V)$ = total macroscopic cross section at V

$\sigma_t^g$ = total macroscopic cross section at group g

$\sigma_s(\Omega', V'; \Omega, V)$ = macroscopic differential scattering cross section from $(\Omega', V')$ to $(\Omega, V)$ per unit V and per unit solid angle at $\Omega$

$\sigma_{s\ell}^{g'\to g}$ = macroscopic differential scattering cross section of moment $\ell$ scattering from group g' to group g

$\chi_1$ = radiation incident toward the right

$\chi_1'$ = radiation transmitted toward the right of the 1st slab

$\chi_2$ = radiation transmitted toward the left

$\chi_2'$ = radiation incident toward the left of the 1st slab

$\phi(x, \omega, V)$ = neutron flux density at $(x, \omega, V)$ per unit V per unit solid angle

$\underline{\phi}^{pt}_{\ell,f}$ = radiation of the $\ell$th moment in the forward direction through the shield due to point isotropic source

$\underline{\phi}^{pt}_{\ell,b}$ = radiation of the $\ell$th moment in the backward direction through the shield due to point isotropic source

# I. INTRODUCTION

The basic objective of radiation shielding is for adequate protection of personnel, equipment, and structures against the harmful effects of nuclear radiation. The shield moderates and absorbs neutrons and gamma rays, the two most important types of radiation from a shielding standpoint.

For shield calculations, there are two general classes of computational estimates: the rough and simple type computations and the elaborate calculations requiring high-speed digital computers. In order to minimize radiation effects, the fine detail of shield design based on the elaborate calculations using high-speed computers is necessary.

One accurate computing technique is the transfer matrix method. The general idea of this method is that the transmission and reflection properties of a shield can be described by matrices which give the outgoing angular and energy distributions in terms of the incoming distributions. The major computational advantage is that various intermediate results are common to problems for different spatial configurations. This indicates that the method is best suited for extensive computational programs.

Because of the importance of the neutron shield and the nature of neutron cross sections, neutron transport calculations were chosen for the present work. However, the same technique can be applied to gamma ray transport calculations.

The angle-energy correlation and the cross sections approximated by the ultra-fine group "point data" have been used for the transfer matrix calculations. Since most of cross section sets developed recently for transport codes are multigroups, the modification of the transfer matrix to accept these cross section sets is required. This problem is solved by using Legendre polynomial expansions in differential scattering cross sections.

By means of the point matrix kernel concept, the modified transfer matrix can be applied to perform point isotropic source analysis without losing its computational advantage. The higher order Legendre moments of the point matrix kernel are also determined such that the outgoing angular and energy distributions can be obtained.

Thus, the purposes of this investigation are

(1) to investigate the applicability of the modified transfer matrix to neutron transport,

(2) to varify the accuracy of the available neutron cross section sets, DLC-2/100G, for use in transport calculations of deep penetration, and

(3) to calculate the angular distributions through the shield materials due to a point isotropic source.

## II. LITERATURE REVIEW

There are several numerical methods dealing with the solution of the Boltzmann transport equation. This is necessary for the solution of the neutron and gamma-ray transport problems. Because of its difficult nature the transport equation is often solved by postulating an approximate form for the solution itself.

A standard one-group time- and azimuthal-independent transport equation with isotropic scattering was solved analytically by Case and Zweifel [7]. They found that there are at most two eigenvalues outside the interval [-1, 1] which correspond to two regular eigenfunctions. The interval [-1, 1] forms the continuous part of the eigenvalue spectrum, for which no exact solutions within Hilbert space $L^2(-1, 1)$ exists. Two kinds of eigenmode expansions are employed such that the eigenvalue spectrum becomes purely discrete; the former continuous part is replaced by a finite set of eigenvalues.

The first approximation is based on the spherical harmonics expansion. The basis of the method is the expansion of all functions of the angular variable in terms of the spherical harmonics [8, 25, 28]. For azimuthal-independent problems, a subset of the spherical harmonics, the Legendre polynomials, suffices. The flux in the Boltzmann equation is expanded in terms of these polynomials. The angular variable from the resulting set of equations is eliminated which leads to a set of coupled differential equations. The fundamental weakness of the spherical harmonics method is that near strong discontinuities in material properties it requires many harmonics to represent the angular

distribution. This deficiency has been improved by using two series of Legendre polynomials to approximate the angular distributions at an interface between two media [8, 25, 28]. This is the so-called double-$P_N$ approximation. In the consistent $P_N$ approximation (PNMG), the energy variable is treated to the same degree of approximation for higher orders of N. Each order of the Legendre expansion retained requires an analogous treatment of its scattering integral. This method has been used extensively in shielding calculation using the $P_3$ expansion [26].

A second approximation is called the discrete ordinate method [8, 25, 28]. The basic idea in this method is to approximate the integral in the Boltzmann equation by a Gauss quadrature formula. It turns out that the resulting numerical accuracy is almost identical to that of the spherical harmonics solution for equivalent computation work. In Carlson's $S_N$ method [5, 25], the integral in the transport equation is approximated by a much simpler device of dividing the angular interval [-1, 1] into finite subintervals and by assuming that the angular distribution varies linearly in each subinterval. This method, in particular the discrete $S_N$ approximation is suitable for high-speed computer calculations.

The invariant imbedding method has been applied to neutron shielding problems [4, 19]. The method depends upon the radiation flux crossing the boundaries of a region and how this radiation flux varies as the thickness of the region changes. The computational advantages of this method are a direct consequence of the fact that the method leads to

an initial value problem rather than the linear boundary value problem obtained by the Boltzmann equation approach.

The Monte Carlo method [25] is based upon statistical analysis and the life histories of a large number of particles released from a source. At each step, collision, absorption, etc., is chosen using a random variable from a known probability distribution for that event.

Direct numerical integration of the Boltzmann equation has been considered [23]. The main difficulty with this method is that it requires a large number of spatial points and angular terms for deep penetration calculations.

The moments method is an expansion technique for solving the transport equation in infinite homogeneous media. The angle, space, and energy variations are treated by polynomial expansion [8, 25]. The method has been applied successfully in the development of buildup factors for gamma-ray shielding calculation [12].

A neatly condensed presentation incorporating a wide range of generalizations of the discrete-angle procedure can be recognized in the transfer matrix formulation. Peebles and Plesset [22] computed the transmission matrix for thin slabs by orders of scattering. They did the spatial integrations analytically and the angle-energy integration numerically. Kataoka [14] developed another approach by using Monte Carlo methods to compute the transmission and reflection matrices for thin slabs. Aronson et al. [1, 2, 3, 6, 29] have developed a formal solution of the differential equation for the transfer matrix as a function of thickness. A polynomial expansion method for the transfer matrix starting from the transport equation was used to

calculate gamma-ray transport [20]. Two dimensional neutron transport based on the transfer matrix method has also been developed [10]. Because of the restriction on a plane source for the transfer matrix method, Rohach [24] developed the point matrix kernel and applied it to the point source analysis.

In the formulation of $\alpha$ and $\beta$ operator matrices in the transfer matrix method, the angle-energy correlation was used in the neutron calculation [3, 29]. Both $\alpha$ and $\beta$ matrices obtained by this technique are not suitable for using recently developed neutron cross section data such as DLC-2/100G. In order to use this data set a reformulation of $\alpha$ and $\beta$ was necessary.

In addition, no work has been done to obtain the angular flux for a point source based on the point matrix kernel. This problem can be solved if the higher order Legendre moments can be determined for the point source geometry.

## III. GENERAL THEORY

### A. Transfer Matrix H Formulation

Consider a sourceless homogeneous slab as shown in Fig. 1. Let the distribution of radiation incident from the left be denoted by $\chi_1$, and that from the right by $\chi_2'$. These distributions are in general functions of direction and energy. Let the distribution emerging to the right be designated by $\chi_1'$ and that to the left by $\chi_2$.

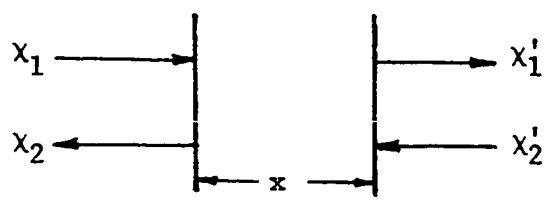


Fig. 1. Slab geometry

The flux vectors obey the matrix equation

$$\begin{bmatrix} \chi_1' \\ \chi_2' \end{bmatrix} = H(x) \begin{bmatrix} \chi_1 \\ \chi_2 \end{bmatrix}, \tag{1}$$

where H(x) is a 2 × 2 matrix of operators.

$$H(x) = \begin{bmatrix} T(x) - R(x)T^{-1}(x)R(x) & R(x)T^{-1}(x) \\ -T^{-1}(x)R(x) & T^{-1}(x) \end{bmatrix}. \tag{2}$$

Here T(x) and R(x) are the transmission matrix operator and the reflection matrix operator, respectively.

Equation (1) leads immediately to a composition law for H-matrices. Consider a two-layer configuration, one has

$$\begin{bmatrix} X_1'' \\ \\ X_2'' \end{bmatrix} = H_2 \begin{bmatrix} X_1' \\ \\ X_2' \end{bmatrix} = H_2 H_1 \begin{bmatrix} X_1 \\ \\ X_2 \end{bmatrix},$$

where $H_1$ and $H_2$ are respectively the H-matrices for slabs 1 and 2. If the H-matrix for the entire configuration is denoted by H, then $H = H_2 H_1$.

The composition of n layers evidently gives

$$H = H_n \cdots H_2 H_1 . \tag{3}$$

From Eq. (3) and the explicit form, Eq. (2), for H, one derives for two layers

$$T = T_2 (I - R_1 R_2)^{-1} T_1 = T_2 \sum_{n=0}^{\infty} (R_1 R_2)^n T_1$$

$$R = R_1 + T_1 (I - R_2 R_1)^{-1} R_2 T_1$$

$$= R_1 + T_1 R_2 (I - R_1 R_2)^{-1} T_1$$

$$= R_1 + T_1 R_2 \sum_{n=1}^{\infty} (R_1 R_2)^n T_1 .$$

where I is the unit operator.

As shown in Ref. [3, 29], the transfer matrix H has the form

$$H(x) = e^{-Wx} . \tag{4}$$

Here W is a 2 X 2 matrix of operators independent of x.

Assume that the transmission operator T(x) and the reflection operator R(x) can be expanded as follows:

$$T(x) = e^{-\alpha x} = I - \alpha x + \frac{1}{2!} (\alpha x)^2 - \cdots \tag{5}$$

$$R(x) = I - e^{-\beta x} = \beta x - \frac{1}{2!} (\beta x)^2 + \cdots \tag{6}$$

Substituting Eqs. (5) and (6) into Eq. (2), to first order in the thickness x, one finds that

$$W = \begin{bmatrix} \alpha & -\beta \\ \beta & -\alpha \end{bmatrix} . \tag{7}$$

It turns out best for purposes of computation to diagonalize W and simultaneously, H. If $\bar{W} = SWS^{-1}$ is diagonal, then

$$H(x) = S^{-1}(e^{-\bar{W}x})S = S^{-1}(e^{-SWS^{-1}x})S.$$

The technique to diagonalize the transfer matrix H(x) is given in Ref. [3, 29]. The results are

$$H(x) = \frac{1}{4}\begin{bmatrix} B_+ & B_- \\ B_- & B_+ \end{bmatrix}\begin{bmatrix} e^{-\Lambda x} & 0 \\ 0 & e^{\Lambda x} \end{bmatrix}\begin{bmatrix} C_+ & C_- \\ C_- & C_+ \end{bmatrix}$$

$$= \frac{1}{4}\begin{bmatrix} B_+e^{-\Lambda x}C_+ + B_-e^{\Lambda x}C_- & B_+e^{-\Lambda x}C_- + B_-e^{\Lambda x}C_+ \\ B_-e^{-\Lambda x}C_+ + B_+e^{\Lambda x}C_- & B_-e^{-\Lambda x}C_- + B_+e^{\Lambda x}C_+ \end{bmatrix} . \tag{8}$$

Due to downscattering only the matrices $B_+$, $B_-$, $C_+$, and $C_-$ are block lower triangular matrices and $\Lambda$ is a diagonal matrix.

## B. Matrix Representation of $\alpha$ and $\beta$

The one dimensional time-independent Boltzmann transport equation can be written

$$\omega \frac{\partial}{\partial x}\phi(x, \omega, V) + \sigma_t(V)\phi(x, \omega, V) = \int_{-1}^{1} d\omega' \int_0^V dV' \int_0^{2\pi}$$

$$d\zeta' \sigma_s(\Omega', V'; \Omega, V)\phi(x, \omega, V').$$

Based on this equation, $\alpha$ and $\beta$ are determined as the integral operators [3, 29],

$$\alpha = \frac{1}{\omega}\int_0^1 d\omega' \left\{\sigma_t(V')\delta(\omega - \omega')\delta(V - V') - \int_0^V dV' \int_0^{2\pi} d\zeta' \sigma_s(\mu_o, V'; V)\right\} \tag{9}$$

$$\beta = \frac{1}{\omega}\int_0^1 d\omega' \int_0^V dV' \int_0^{2\pi} d\zeta' \sigma_s(\mu_o', V'; V), \tag{10}$$

where

$$\mu_o = \omega\omega' + (1 - \omega^2)^{1/2}(1 - \omega'^2)^{1/2} \cos\zeta'$$

$$\mu_o' = -\omega\omega' + (1 - \omega^2)^{1/2}(1 - \omega'^2)^{1/2} \cos\zeta'.$$

The differential scattering cross section in Eqs. (9) and (10) can be expanded in Legendre polynomials [16],

$$\sigma_s(\mu_o, V'; V) = \sum_{\ell=0}^{\infty} \frac{2\ell + 1}{4\pi} \sigma_{s\ell}(V'; V) P_\ell(\mu_o). \tag{11}$$

Substitution of Eq. (11) into Eqs. (9) and (10) will result in

$$\alpha = \frac{1}{\omega}\int_0^1 d\omega' \left\{\sigma_t(V')\delta(\omega - \omega')\delta(V - V') - \int_0^V dV' \int_0^{2\pi} d\zeta' \sum_{\ell=0}^{\infty} \frac{2\ell + 1}{4\pi} \sigma_{s\ell}(V'; V) P_\ell(\mu_o)\right\} \tag{12}$$

$$\beta = \frac{1}{\omega}\int_0^1 d\omega' \int_0^V dV' \int_0^{2\pi} d\zeta' \sum_{\ell=0}^{\infty} \frac{2\ell + 1}{4\pi} \sigma_{s\ell}(V'; V) P_\ell(\mu_o'). \tag{13}$$

Using the equations

$$\int_0^{2\pi} d\zeta' P_\ell(\mu_o) = 2\pi P_\ell(\omega) P_\ell(\omega')$$

and

$$\int_0^{2\pi} d\zeta' P_\ell(\mu_o') = 2\pi P_\ell(\omega) P_\ell(-\omega'),$$

Equations (12) and (13) become

$$\alpha = \frac{1}{\omega} \int_0^1 d\omega' \left\{ \sigma_t(V') \delta(\omega - \omega') \delta(V - V') - \int_0^V dV' \sum_{\ell=0}^{\infty} \frac{2\ell + 1}{2} \sigma_{s\ell}(V'; V) P_\ell(\omega) P_\ell(\omega') \right\} \tag{14}$$

and

$$\beta = \frac{1}{\omega} \int_0^1 d\omega' \int_0^V dV' \sum_{\ell=0}^{\infty} \frac{2\ell + 1}{2} \sigma_{s\ell}(V'; V) P_\ell(\omega) P_\ell(-\omega'). \tag{15}$$

In order to deal with matrices rather than integral operators, a group representation in energy and an angular expansion in half-range Legendre polynomials have been chosen. Expand the flux as

$$\phi(x, \omega, V) = \sum_{n=0}^{\infty} \phi_n(x, V) P_n^+(\omega). \tag{16}$$

Substituting Eq. (16) into Eq. (14) and multiplying both sides by $\omega$, results in

$$\sum_{n=0}^{\infty} \alpha\omega\phi_n(x, V) P_n^+(\omega) = \sum_{n=0}^{\infty} \int_0^1 d\omega' \left\{ \sigma_t(V') \delta(\omega - \omega') \delta(V - V') - \int_0^V dV' \sum_{\ell=0}^{\infty} \frac{2\ell + 1}{2} \sigma_{s\ell}(V'; V) P_\ell(\omega) P_\ell(\omega') \right\} \phi_n(x, V') P_n^+(\omega').$$

Because of the orthogonality of the half- range Legendre polynomials, the above equation can be multiplied by $P_m^+(\omega)$ and integrated over $\omega$. Therefore one has

$$\sum_{n=0}^{\infty} \alpha\phi_n(x, V) \int_0^1 \omega P_n^+(\omega) P_m^+(\omega) d\omega$$

$$= \sum_{n=0}^{\infty} \int_0^1 d\omega \int_0^1 d\omega' \sigma_t(V') \delta(\omega - \omega') \delta(V - V') \phi_n(x, V') P_n^+(\omega') P_m^+(\omega)$$

$$- \sum_{n=0}^{\infty} \int_0^1 d\omega \int_0^1 d\omega' \int_0^V dV' \sum_{\ell=0}^{\infty} \frac{2\ell+1}{2} \sigma_{s\ell}(V'; V) P_\ell(\omega) P_\ell(\omega')$$

$$\phi_n(x, V') P_n^+(\omega') P_m^+(\omega).$$

Define

$$e_{mn} = \int_0^1 \omega P_n^+(\omega) P_m^+(\omega) d\omega, \tag{17}$$

$$d_{mn}^{\ell}(\mu_o) = \int_0^1 d\omega \int_0^1 d\omega' P_\ell(\omega) P_\ell(\omega') P_n^+(\omega') P_m^+(\omega), \tag{18}$$

$$z_{mn} = \int_0^1 d\omega \int_0^1 d\omega' \delta(\omega - \omega') P_n^+(\omega') P_m^+(\omega) = \frac{\delta_{mn}}{2n+1}, \tag{19}$$

then $$\sum_{n=0}^{\infty} e_{mn} \alpha\phi_n(x, V) = \sum_{n=0}^{\infty} z_{mn} \sigma_t(V') \delta(V - V') \phi_n(x, V')$$

$$- \sum_{n=0}^{\infty} \sum_{\ell=0}^{\infty} \frac{2\ell+1}{2} \int_0^V \sigma_{s\ell}(V'; V) d_{mn}^{\ell}(\mu_o) \phi_n(x, V') dV'.$$

To put the equations into matrix form, the angular expansion is truncated after $\ell = L$, and hence $n = L$, resulting in

$$E\alpha\underline{\phi}(x, V) = Z\sigma_t(V') \delta(V - V') \underline{\phi}(x, V')$$

$$- \sum_{\ell=0}^{L} \frac{2\ell+1}{2} \int_0^V \sigma_{s\ell}(V'; V) D_\ell(\mu_o) \underline{\phi}(x, V') dV'. \tag{20}$$

The $\beta$ operator is also readily identified in matrix form as

$$E\beta\underline{\phi}(x, V) = \sum_{\ell=0}^{L} \frac{2\ell+1}{2} \int_0^V \sigma_{s\ell}(V'; V) D_\ell(\mu_o') \underline{\phi}(x, V') dV', \quad (21)$$

where

$$D_\ell(\mu_o') = (-1)^\ell D_\ell(\mu_o)$$

The computations of E, $D_\ell(\mu_o)$, and $D_\ell(\mu_o')$ are given in Appendix.

The energy variable is approximated by the multigroup formulation. Define the gth group as $\Delta V_g = V_{g+1} - V_g$. In the neutron calculation V stands for lethargy and the first group is the lowest lethargy group. The neutron flux and cross sections are assumed constant within each group. Equations (20) and (21) are then integrated over the gth group using the lethargy variable as the integration parameter.

$$E \int_{V_g}^{V_{g+1}} \alpha_{g'} \underline{\phi}(x, V) dV = Z \int_{V_g}^{V_{g+1}} \sigma_t(V') \delta(V - V') \underline{\phi}(x, V) dV$$
$$- \sum_{\ell=0}^{L} \frac{2\ell+1}{2} \int_{V_g}^{V_{g+1}} dV \int_{V_{g'}}^{V_{g'+1}} \sigma_{s\ell}(V'; V) D_\ell(\mu_o) \underline{\phi}(x, V) dV'. \quad (22)$$

Using the definition

$$\int_{V_g}^{V_{g+1}} \alpha_{g'} \underline{\phi}(x, V) dV \equiv \alpha_{gg'} \underline{\phi}_g(x) \Delta V_g ,$$

where

$$\underline{\phi}_g(x) \Delta V_g = \int_{V_g}^{V_{g+1}} \underline{\phi}(x, V) dV,$$

the operator formulation of Eq. (22) becomes

$$E\alpha_{gg'}\underline{\phi}_g(x)\Delta V_g = Z\sigma_t^g\underline{\phi}_g(x)\delta_{gg'}\Delta V_g - \sum_{\ell=0}^{L}\frac{2\ell+1}{2}\sigma_{s\ell}^{g'\to g}D_\ell(\mu_o)\underline{\phi}_g(x)\Delta V_g\Delta V_{g'},$$

$$\alpha_{gg'} = E^{-1}Z\sigma_t^g\delta_{gg'} - E^{-1}\sum_{\ell=0}^{L}\frac{2\ell+1}{2}\sigma_{s\ell}^{g'\to g}D_\ell(\mu_o)\Delta V_{g'} \quad . \tag{23}$$

Similarly,

$$\beta_{gg'} = E^{-1}\sum_{\ell=0}^{L}\frac{2\ell+1}{2}\sigma_{s\ell}^{g'\to g}D_\ell(\mu_o')\Delta V_{g'} \quad . \tag{24}$$

The existence of $E^{-1}$ for a set of truncated polynomials is shown in Ref. [29]. Thus $\alpha_{gg'}$ and $\beta_{gg'}$ can be calculated by the matrix multiplications.

## C. Determination of the Transmission and Reflection Matrices

By equating Eqs. (2) and (8), the expressions of T(x) and R(x) become

$$T(x) = 4(B_-e^{-\Lambda x}C_+ + B_+e^{\Lambda x}C_+)^{-1}$$

$$R(x) = \frac{1}{4}(B_+e^{-\Lambda x}C_- + B_-e^{\Lambda x}C_+)T(x).$$

Numerically, it is not convenient to work with large positive exponentials. In all practical calculations performed to date, the asymptotic expressions have been applied [24],

$$T_\infty(x) = 4C_+^{-1}e^{-\Lambda x}B_+^{-1} \quad , \tag{25}$$

$$R_\infty(x) = B_-B_+^{-1} \quad . \tag{26}$$

For very thin (1 mean free path or less) shields, the more accurate expression should be used.

## D. Point Matrix Kernel Method

The point matrix kernel is derived from the transfer matrix by using the point-to-plane transformation [24]

$$I_\ell^{p\ell}(x, V) = 2\pi \int_{|x|}^{\infty} r P_\ell(\tfrac{x}{r}) I_\ell^{pt}(r, V)dr, \tag{27}$$

where

$$I_\ell(x, V) = 2\pi \int_{-1}^{1} I(x, V, \omega)P_\ell(\omega)d\omega \tag{28}$$

and

$$I(x, V, \omega) = \sum_{\ell=0}^{\infty} \frac{2\ell+1}{4\pi} I_\ell(x, V)P_\ell(\omega). \tag{29}$$

The integral equation of $I_\ell^{pt}(r, V)$ in Eq. (27) can be solved for each moment. When $\ell = 0$

$$I_0^{p\ell}(x, V) = 2\pi \int_{|x|}^{\infty} r(1) I_0^{pt}(r, V)dr,$$

taking the partial derivative with respect to x and assuming that the flux at the infinite distance is zero results in

$$\frac{\partial}{\partial x} I_0^{p\ell}(x, V) = - 2\pi x I_0^{pt}(x, V),$$

or

$$I_0^{pt}(x, V) = - \frac{1}{2\pi x^2} \left\{ x \frac{\partial}{\partial x} I_0^{p\ell}(x, V) \right\}. \tag{30}$$

When $\ell = 1$

$$I_1^{p\ell}(x, V) = 2\pi \int_{|x|}^{\infty} r(\tfrac{x}{r}) I_1^{pt}(r, V)dr,$$

using the same technique as in $\ell = 0$ results in

$$\frac{\partial}{\partial x} I_1^{p\ell}(x, V) = \frac{1}{x} I_1^{p\ell}(x, V) - 2\pi x I_1^{pt}(x, V),$$

or
$$I_1^{pt}(x, V) = -\frac{1}{2\pi x^2}\left\{x \frac{\partial}{\partial x} I_1^{p\ell}(x, V) - I_1^{p\ell}(x, V)\right\}. \tag{31}$$

For $\ell = 2$

$$I_2^{p\ell}(x, V) = 2\pi \int_{|x|}^{\infty} r\left(\frac{3}{2}\frac{x^2}{r^2} - \frac{1}{2}\right) I_2^{pt}(r, V)dr,$$

after taking the partial derivative twice one has

$$\frac{\partial^2}{\partial x^2} I_2^{p\ell}(x, V) = \frac{1}{x}\frac{\partial}{\partial x} I_2^{p\ell}(x, V) - 6\pi I_2^{pt}(x, V) - 2\pi x \frac{\partial}{\partial x} I_2^{pt}(x, V).$$

In order to obtain $I_2^{pt}(x, V)$ as an exact differential, the above equation can be multiplied by $x^2$. This results in

$$2\pi \frac{\partial}{\partial x} x^3 I_2^{pt}(x, V) = -x^2 \frac{\partial^2}{\partial x^2} I_2^{p\ell}(x, V) + x \frac{\partial}{\partial x} I_2^{p\ell}(x, V). \tag{32}$$

After integration by parts, Eq. (32) becomes

$$I_2^{pt}(x, V) = -\frac{1}{2\pi x^2}\left\{x \frac{\partial}{\partial x} I_2^{p\ell}(x, V) - 3I_2^{p\ell}(x, V) + 3x^{-1}\int_0^x I_2^{p\ell}(x, V)dx\right\}. \tag{33}$$

For $\ell = 3$

$$I_3^{p\ell}(x, V) = 2\pi \int_{|x|}^{\infty} r\left(\frac{5}{2}\frac{x^3}{r^3} - \frac{3}{2}\frac{x}{r}\right) I_3^{pt}(r, V)dr,$$

because of only two integration terms involving $I_3^{pt}(r, V)$, again second order partial derivatives are required. The result is

$$\frac{\partial^2}{\partial x^2} I_3^{p\ell}(x, V) = \frac{3}{x} \frac{\partial}{\partial x} I_3^{p\ell}(x, V) - \frac{3}{x^2} I_3^{p\ell}(x, V) - 8\pi I_3^{p\ell}(x, V)$$

$$- 2\pi x \frac{\partial}{\partial x} I_3^{pt}(x, V). \tag{34}$$

An exact differential form of $I_3^{pt}(x, V)$ can be obtained by multiplying by $x^3$ in the above equation and writing

$$2\pi \frac{\partial}{\partial x} x^4 I_3^{pt}(x, V) = - x^3 \frac{\partial^2}{\partial x^2} I_3^{p\ell}(x, V) + 3x^2 \frac{\partial}{\partial x} I_3^{p\ell}(x, V)$$

$$- 3x I_3^{p\ell}(x, V). \tag{35}$$

Equation (35) can be solved for $I_3^{pt}(x, V)$ by integration by parts,

$$I_3^{pt}(x, V) = - \frac{1}{2\pi x^2} \left\{ x \frac{\partial}{\partial x} I_3^{p\ell}(x, V) - 6 I_3^{p\ell}(x, V) \right.$$

$$\left. + 15 x^{-1} \int_0^x I_3^{p\ell}(x, V) dx - 15 x^{-2} \iint I_3^{p\ell}(x, V) dx^2 \right\}. \tag{36}$$

For $\ell = 4$ and $\ell = 5$, one has

$$I_4^{p\ell}(x, V) = 2\pi \int_{|x|}^{\infty} r \left( \frac{35}{8} \frac{x^4}{r^4} - \frac{30}{8} \frac{x^2}{r^2} + \frac{3}{8} \right) I_4^{pt}(r, V) dr$$

and

$$I_5^{p\ell}(x, V) = 2\pi \int_{|x|}^{\infty} r \left( \frac{63}{8} \frac{x^5}{r^5} - \frac{70}{8} \frac{x^3}{r^3} + \frac{15}{8} \frac{x}{r} \right) I_5^{pt}(r, V) dr,$$

taking partial derivatives three times is necessary for both equations and the results are

$$\frac{\partial^3}{\partial x^3} I_4^{p\ell}(x, V) = \frac{3}{x} \frac{\partial^2}{\partial x^2} I_4^{p\ell}(x, V) - \frac{3}{x^2} \frac{\partial}{\partial x} I_4^{p\ell}(x, V) - \frac{30\pi}{x} I_4^{pt}(x, V)$$

$$- 18\pi \frac{\partial}{\partial x} I_4^{pt}(x, V) - 2\pi x \frac{\partial^2}{\partial x^2} I_4^{pt}(x, V)$$

and $$\frac{\partial^3}{\partial x^3} I_5^{p\ell}(x, V) = \frac{6}{x} \frac{\partial^2}{\partial x^2} I_5^{p\ell}(x, V) - \frac{15}{x^2} \frac{\partial}{\partial x} I_5^{p\ell}(x, V) + \frac{15}{x^5} I_5^{p\ell}(x, V)$$
$$- \frac{48\pi}{x} I_5^{pt}(x, V) - 22\pi \frac{\partial}{\partial x} I_5^{pt}(x, V) - 2\pi x \frac{\partial^2}{\partial x^2} I_5^{pt}(x, V).$$

Multiplying the equations by $x^5$ and $x^6$, respectively, exact differential forms can be obtained. These are

$$2\pi \frac{\partial}{\partial x} (x^3 I_4^{pt}(x, V)) = - x^5 \frac{\partial^3}{\partial x^3} I_4^{p\ell}(x, V) + 3x^4 \frac{\partial^2}{\partial x^2} I_4^{p\ell}(x, V)$$
$$- 3x^3 \frac{\partial}{\partial x} I_4^{p\ell}(x, V)$$

and $$2\pi \frac{\partial}{\partial x} (x^3 \frac{\partial}{\partial x} x^4 I_5^{pt}(x, V)) = - x^6 \frac{\partial^3}{\partial x^3} I_5^{p\ell}(x, V) + 6x^5 \frac{\partial^2}{\partial x^2} I_5^{p\ell}(x, V)$$
$$- 15x^4 \frac{\partial}{\partial x} I_5^{p\ell}(x, V) + 15x^3 I_5^{p\ell}(x, V).$$

After the integrations one has

$$I_4^{pt}(x, V) = - \frac{1}{2\pi x^2} \left\{ x \frac{\partial}{\partial x} I_4^{p\ell}(x, V) - 10 I_4^{p\ell}(x, V) \right.$$
$$+ 45x^{-1} \int I_4^{p\ell}(x, V)dx - 105x^{-2} \iint I_4^{p\ell}(x, V)dx^2$$
$$\left. + 105x^{-3} \iiint I_4^{p\ell}(x, V)dx^3 \right\}, \tag{37}$$

and $$I_5^{pt}(x, V) = - \frac{1}{2\pi x^2} \left\{ x \frac{\partial}{\partial x} I_5^{p\ell}(x, V) - 15 I_5^{p\ell}(x, V) \right.$$
$$+ 105x^{-1} \int I_5^{p\ell}(x, V)dx - 420\, x^{-2} \iint I_5^{p\ell}(x, V)dx^2$$
$$\left. + 945x^{-3} \iiint I_5^{p\ell}(x, V)dx^3 - 945x^{-4} \iiiint I_5^{p\ell}(x, V)dx^4 \right\}. \tag{38}$$

From Eqs. (30), (31), (33), (36), (37), and (38), one can deduce a general formula for the $\ell$th moment to be

$$I_{\ell}^{pt}(x, V) = -\frac{1}{2\pi x^2} \sum_{k=0}^{\ell} A_{\ell k} x^{1-k} D_x^{1-k} I_{\ell}^{p\ell}(x, V), \tag{39}$$

where $$A_{\ell k} = \frac{(-1)^k(\ell + k)!}{2^k k!(\ell - k)!}$$

$$D_x^{1} I_{\ell}^{p\ell}(x, V) = \frac{\partial}{\partial x} I_{\ell}^{p\ell}(x, V),$$

and $$D_x^{-1} I_{\ell}^{p\ell}(x, V) = \int_0^x I_{\ell}^{p\ell}(x, V)dx, \text{ etc.},$$

Eq. (39) is obtained by deduction only and has not been proven in general.

One can find that $\ell = 0$ and $\ell = 1$ correspond to the flux density and the current density relations.

In an infinite medium, infinite reflection on both sides of the source should be taken into account. Therefore the total source is

$$\left\{(I + R_{\infty}^2 + R_{\infty}^4 + \ldots) + (R_{\infty} + R_{\infty}^3 + \ldots)\right\} \underline{S} = (I - R_{\infty})^{-1} \underline{S}.$$

Similarly, the infinite reflections at the response point result in the same expression. In the forward direction through the shield material,

$$I + R_{\infty}^2 + R_{\infty}^4 + \ldots = (I - R_{\infty}^2)^{-1}$$

and in the backward direction

$$R_{\infty} + R_{\infty}^3 + \ldots = R_{\infty}(I - R_{\infty}^2)^{-1} .$$

Hence $(I - R_{\infty}^2)^{-1} T(x) (I - R_{\infty})^{-1} \underline{S}$ and $R_{\infty}(I - R_{\infty}^2)^{-1} T(x) (I - R_{\infty})^{-1} \underline{S}$ give the distributions in the forward and backward directions through the slab. Applying the point-to-plane transformation to Eq. (39) results in

$$\underline{\phi}^{pt}_{\ell,f} = (I - R_\infty^2)^{-1} \left\{ - \frac{1}{2\pi x^2} \sum_{k=0}^{\ell} A_{\ell k} x^{1-k} D_x^{1-k} T(x) \right\} (I - R_\infty)^{-1} \underline{S}, \tag{40}$$

and

$$\underline{\phi}^{pt}_{\ell,b} = R_\infty (I - R_\infty^2)^{-1} \left\{ - \frac{1}{2\pi x^2} \sum_{k=0}^{\ell} A_{\ell k} x^{1-k} D_x^{1-k} T(x) \right\} (I - R_\infty)^{-1} \underline{S}. \tag{41}$$

An immediate conclusion is that the infinite reflection functions are the same for point and plane and hence transmission through a finite slab can be generalized from Eqs. (40) and (41) to be

$$\underline{\phi}^{pt}_{\ell} = \left\{ - \frac{1}{2\pi x^2} \sum_{k=0}^{\ell} A_{\ell k} x^{1-k} D_x^{1-k} T(x) \right\} \underline{S}. \tag{42}$$

The expression in the braces in Eq. (42) is called the point matrix kernel of the $\ell$th moment. Equation (42) is valid under the assumption that the boundary effects due to boundaries not being normal to the ray are insignificant.

After expanding Eq. (42) one finds that the higher Legendre moment can be developed in terms of the lower moments plus one extra term,

$$\underline{\phi}^{pt}_{\ell} = \sum_{k=0}^{\ell-1} B_{\ell k} \underline{\phi}^{pt}_{k} + \frac{1}{2\pi x^2} B_{\ell\ell} x^{1-\ell} D_x^{1-\ell} T(x) \underline{S}, \tag{43}$$

where the $B_{\ell k}$'s are constants determined by $A_{\ell k}$. In Table 1 are shown values of $B_{\ell k}$ with $\ell$ up to 6.

In both Eqs. (42) and (43), the derivative and integrations of T(x) are required, the asymptotic expression $T_\infty(x)$ has been used for this derivation. Therefore

Table 1. Values of $B_{\ell k}$

| $\ell$ | k value | | | | | | |
|---|---|---|---|---|---|---|---|
| | 0 | 1 | 2 | 3 | 4 | 5 | 6 |
| 0 | - 1 | 0 | 0 | 0 | 0 | 0 | 0 |
| 1 | 1 | 1 | 0 | 0 | 0 | 0 | 0 |
| 2 | - 2 | 3 | - 3 | 0 | 0 | 0 | 0 |
| 3 | 5 | - 9 | 5 | 15 | 0 | 0 | 0 |
| 4 | - 14 | 28 | - 20 | 7 | - 105 | 0 | 0 |
| 5 | 42 | - 90 | 75 | - 35 | 9 | 945 | 0 |
| 6 | - 132 | 297 | - 275 | 154 | - 54 | 11 | - 10395 |

$$xD_x^1 T_\infty(x) = 4C_+^{-1}\left\{(-\Lambda x)e^{-\Lambda x} B_+^{-1}\right\}, \tag{44}$$

$$x^{-1}D_x^{-1}T_\infty(x) = 4C_+^{-1}\left\{-(\Lambda x)^{-1}e^{-\Lambda x} + (\Lambda x)^{-1}\right\} B_+^{-1},$$

$$x^{-2}D_x^{-2}T_\infty(x) = 4C_+^{-1}\left\{(\Lambda x)^{-2}e^{-\Lambda x} - (\Lambda x)^{-2} + \frac{1}{1!}(\Lambda x)^{-1}\right\} B_+^{-1},$$

and the general expression for the integration of $T_\infty(x)$ is

$$x^{-n}D_x^{-n}T_\infty(x) = 4C_+^{-1}(-1)^n\left\{(\Lambda x)^{-n}e^{-\Lambda x} - (\Lambda x)^{-n} + \frac{1}{1!}(\Lambda x)^{-n+1}\right.$$

$$\left. - \frac{1}{2!}(\Lambda x)^{-n+2} + \ldots + \frac{1}{(n-1)!}(\Lambda x)^{-1}\right\} B_+^{-1}. \tag{45}$$

# IV. COMPUTATIONAL METHODS AND NUMERICAL INVESTIGATIONS

Based on the theory discussed previously, a computer code has been developed such that the necessary operations in the transfer matrix method can be performed effectively and efficiently. The code is divided into four steps.

In the first step the two basic matrix operators $\alpha_{gg'}$ and $\beta_{gg'}$ defined in Eqs. (23) and (24) are calculated. The second step is used to diagonalize the matrix W, given in Eq. (7). In this procedure eigenvalues and eigenvectors of very large matrices must be found. In step three, the $B_{\pm}$ and $C_{\pm}$ matrices are obtained. Further manipulations of these matrices are done for future shielding calculations. In step four, the basic shielding calculations are performed.

The input cross sections are obtained from DLC-2/100G[1]. These data are averaged over each specified group width and consist of fine group constants. The data have a 100-group structure with energy boundaries identical to those in the GAM-II library [13], as shown in Table 2. The group-to-group transfer matrices reflects only down-scatter in energy, and group 100 serves as a thermal group. In most of the cross section data files the microscopic cross sections are arranged in the following format:

---

[1]DLC-2/100G, a 100-group neutron transport code cross section data generated by SUPERTOG from ENDF/B-III, was generated by R. Q. Wright of the ORNL Mathematical Division and distributed by RSIC, Oak Ridge, Tennessee.

Table 2. GAM-II energy group boundaries

| Group | Energy | | Velocity |
|---|---|---|---|
| | Upper (ev) | Lower (ev) | (cm/sec) |
| 1 | 1.4918(7)[a] | 1.3499(7) | 5.1555(9) |
| 2 | 1.3499(7) | 1.2214(7) | 4.9093(9) |
| 3 | 1.2214(7) | 1.1052(7) | 4.6744(9) |
| 4 | 1.1052(7) | 1.0000(7) | 4.4503(9) |
| 5 | 1.0000(7) | 9.0484(6) | 4.2366(9) |
| 6 | 9.0484(6) | 8.1873(6) | 4.0328(9) |
| 7 | 8.1873(6) | 7.4082(6) | 3.8386(9) |
| 8 | 7.4082(6) | 6.7032(6) | 3.6536(9) |
| 9 | 6.7032(6) | 6.0653(6) | 3.4772(9) |
| 10 | 6.0653(6) | 5.4881(6) | 3.3092(9) |
| 11 | 5.4881(6) | 4.9659(6) | 3.1492(9) |
| 12 | 4.9659(6) | 4.4933(6) | 2.9968(9) |
| 13 | 4.4933(6) | 4.0657(6) | 2.8517(9) |
| 14 | 4.0657(6) | 3.6788(6) | 2.7135(9) |
| 15 | 3.6788(6) | 3.3287(6) | 2.5819(9) |
| 16 | 3.3287(6) | 3.0119(6) | 2.4566(9) |
| 17 | 3.0119(6) | 2.7253(6) | 2.3374(9) |
| 18 | 2.7253(6) | 2.4660(6) | 2.2239(9) |
| 19 | 2.4660(6) | 2.2313(6) | 2.1158(9) |
| 20 | 2.2313(6) | 2.0190(6) | 2.0130(9) |
| 21 | 2.0190(6) | 1.8268(6) | 1.9151(9) |
| 22 | 1.8268(6) | 1.6530(6) | 1.8220(9) |
| 23 | 1.6530(6) | 1.4957(6) | 1.7333(9) |
| 24 | 1.4957(6) | 1.3534(6) | 1.6490(9) |
| 25 | 1.3534(6) | 1.2246(6) | 1.5688(9) |
| 26 | 1.2246(6) | 1.1080(6) | 1.4924(9) |
| 27 | 1.1080(6) | 1.0026(6) | 1.4197(9) |
| 28 | 1.0026(6) | 9.0719(5) | 1.3506(9) |
| 29 | 9.0719(5) | 8.2086(5) | 1.2848(9) |
| 30 | 8.2086(5) | 7.4274(5) | 1.2222(9) |
| 31 | 7.4274(5) | 6.7206(5) | 1.1627(9) |
| 32 | 6.7206(5) | 6.0811(5) | 1.1061(9) |
| 33 | 6.0811(5) | 5.5024(5) | 1.0522(9) |
| 34 | 5.5024(5) | 4.9788(5) | 1.0009(9) |
| 35 | 4.9788(5) | 4.5050(5) | 9.5210(8) |
| 36 | 4.5050(5) | 4.0763(5) | 9.0571(8) |
| 37 | 4.0763(5) | 3.6884(5) | 8.6160(8) |
| 38 | 3.6884(5) | 3.3374(5) | 8.1961(8) |
| 39 | 3.3374(5) | 3.0198(5) | 7.7965(8) |
| 40 | 3.0198(5) | 2.7324(5) | 7.4169(8) |
| 41 | 2.7324(5) | 2.4724(5) | 7.0549(8) |

[a] 1.4918(7) means $1.4918 \times 10^7$.

Table 2. (Continued)

| Group | Energy | | Velocity |
|---|---|---|---|
| | Upper (ev) | Lower (ev) | (cm/sec) |
| 42 | 2.4724(5) | 2.2371(5) | 6.7109(8) |
| 43 | 2.2371(5) | 2.0242(5) | 6.3840(8) |
| 44 | 2.0242(5) | 1.8316(5) | 6.0726(8) |
| 45 | 1.8316(5) | 1.6573(5) | 5.7761(8) |
| 46 | 1.6573(5) | 1.4996(5) | 5.4957(8) |
| 47 | 1.4996(5) | 1.3569(5) | 5.2269(8) |
| 48 | 1.3569(5) | 1.2278(5) | 4.9716(8) |
| 49 | 1.2278(5) | 1.1109(5) | 4.7286(8) |
| 50 | 1.1109(5) | 8.6519(4) | 4.3476(8) |
| 51 | 8.6519(4) | 6.7381(4) | 3.8368(8) |
| 52 | 6.7381(4) | 5.2476(4) | 3.3859(8) |
| 53 | 5.2476(4) | 4.0869(4) | 2.9881(8) |
| 54 | 4.0869(4) | 3.1829(4) | 2.6370(8) |
| 55 | 3.1829(4) | 2.4788(4) | 2.3271(8) |
| 56 | 2.4788(4) | 1.9305(4) | 2.0537(8) |
| 57 | 1.9305(4) | 1.5035(4) | 1.8124(8) |
| 58 | 1.5035(4) | 1.1709(4) | 1.5994(8) |
| 59 | 1.1709(4) | 9.1191(3) | 1.4115(8) |
| 60 | 9.1191(3) | 7.1020(3) | 1.2456(8) |
| 61 | 7.1020(3) | 5.5310(3) | 1.0993(8) |
| 62 | 5.5310(3) | 4.3076(3) | 9.7009(7) |
| 63 | 4.3076(3) | 3.3547(3) | 8.5610(7) |
| 64 | 3.3547(3) | 2.6127(3) | 7.5551(7) |
| 65 | 2.6127(3) | 2.0348(3) | 6.6674(7) |
| 66 | 2.0348(3) | 1.5847(3) | 5.8839(7) |
| 67 | 1.5847(3) | 1.2341(3) | 5.1925(7) |
| 68 | 1.2341(3) | 9.6115(2) | 4.5824(7) |
| 69 | 9.6115(2) | 7.4855(2) | 4.0440(7) |
| 70 | 7.4855(2) | 5.8297(2) | 3.5688(7) |
| 71 | 5.8297(2) | 4.5402(2) | 3.1494(7) |
| 72 | 4.5402(2) | 3.5359(2) | 2.7794(7) |
| 73 | 3.5359(2) | 2.7538(2) | 2.4528(7) |
| 74 | 2.7538(2) | 2.1446(2) | 2.1646(7) |
| 75 | 2.1446(2) | 1.6702(2) | 1.9102(7) |
| 76 | 1.6702(2) | 1.3008(2) | 1.6858(7) |
| 77 | 1.3008(2) | 1.0131(2) | 1.4877(7) |
| 78 | 1.0131(2) | 7.8897(1) | 1.3129(7) |
| 79 | 7.8897(1) | 6.1445(1) | 1.1586(7) |
| 80 | 6.1445(1) | 4.7854(1) | 1.0225(7) |
| 81 | 4.7854(1) | 3.7268(1) | 9.0234(6) |
| 82 | 3.7268(1) | 2.9025(1) | 7.9631(6) |
| 83 | 2.9025(1) | 2.2604(1) | 7.0274(6) |
| 84 | 2.2604(1) | 1.7604(1) | 6.2017(6) |

Table 2. (Continued)

| Group | Energy | | Velocity |
|---|---|---|---|
| | Upper (ev) | Lower (ev) | (cm/sec) |
| 85 | 1.7604(1) | 1.3710(1) | 5.4729(6) |
| 86 | 1.3710(1) | 1.0678(1) | 4.8299(6) |
| 87 | 1.0678(1) | 8.3157(0) | 4.2623(6) |
| 88 | 8.3157(0) | 6.4763(0) | 3.7615(6) |
| 89 | 6.4763(0) | 5.0438(0) | 3.3195(6) |
| 90 | 5.0438(0) | 3.9281(0) | 2.9295(6) |
| 91 | 3.9281(0) | 3.0592(0) | 2.5852(6) |
| 92 | 3.0592(0) | 2.3825(0) | 2.2815(6) |
| 93 | 2.3825(0) | 1.8555(0) | 2.0134(6) |
| 94 | 1.8555(0) | 1.4451(0) | 1.7768(6) |
| 95 | 1.4451(0) | 1.1254(0) | 1.5680(6) |
| 96 | 1.1254(0) | 8.7649(-1) | 1.3838(6) |
| 97 | 8.7649(-1) | 6.8262(-1) | 1.2212(6) |
| 98 | 6.8262(-1) | 5.3163(-1) | 1.0777(6) |
| 99 | 5.3163(-1) | 4.1404(-1) | 9.5108(5) |
| 100 | 4.1404(-1) | 3.8745(-14) | 6.2932(5) |

| Position | Cross section type | |
|---|---|---|
| 1 | $\sigma_{act}$ | |
| . | $\sigma_{act}$ | |
| . | $\sigma_{act}$ | |
| IHT - 2 | $\sigma_a$ | |
| IHT - 1 | $\nu\sigma_f$ | |
| IHT | $\sigma_t$ | |
| IHT + 1 | $\sigma_{s\ell}^{g+NUS\rightarrow g}$ | upscatter |
| . | . | |
| . | . | |
| IHS - 1 | $\sigma_{s\ell}^{g+1\rightarrow g}$ | |
| IHS | $\sigma_{s\ell}^{g\rightarrow g}$ | |
| IHS + 1 | $\sigma_{s\ell}^{g-1\rightarrow g}$ | downscatter |
| . | . | |
| . | . | |
| IHM | $\sigma_{s\ell}^{g-NDS\rightarrow g}$ | |

Thus the parameters IHT, IHS, and IHM completely describe the format of the cross sections. If there is no activity and no upscatter cross sections, IHT = 3 and IHS = IHT + 1 will be used. On the DLC-2/100G file, IHT = 3, IHS = 4, and IHM = 103. Legendre polynomial expansions for cross sections are in increasing order ($P_0$, $P_1$, etc.).

For the order of $P_\ell$ larger than zero, only the first IHN terms are nonzero and the rest, IHM - IHN, are zero. Computational time can be reduced by using IHM as the length of the cross section table for the $P_0$ term and using IHN for those with orders higher than $P_0$.

Because of downscatter, the matrices $\alpha$ and $\beta$ have the characteristic block lower triangular form. The number of diagonal blocks depends on the number of energy groups used in the calculations. Each block is a square matrix and represents the number of Legendre terms used in the angular expansion. The matrices, $E^{-1}$, $E^{-1}Z$, and $D_\ell(\mu_o)$, are stored as one-dimensional arrays with a vector serving as the locator of the first entry of each block matrix. Scattering cross sections are read in such that $\sigma_{so}^{g'\to g}$, ..., $\sigma_{sL}^{g'\to g}$ are formed as the diagonal matrix located at the (g', g) block. Thus $\alpha_{gg'}$ and $\beta_{gg'}$ can be calculated by the matrix multiplications.

The diagonalization of W in step two can be reduced to that of the operator $A = (\alpha + \beta)(\alpha - \beta)$. Eigenvalues and dual eigenvectors in each diagonal block of A are computed first by IMSL subroutines[1]. By means of these results, the eigenvalue spectrum and dual eigenvector matrices of the block triangular matrix A can be computed [3, 29].

The $\alpha$ and $\beta$ matrices along with eigenvalue and dual eigenvector matrices are read into the third step to compute the matrices $B_{\pm}$ and $C_{\pm}$. In order to facilitate further shielding calculations, five combinations $B_+^{-1}$, $C_+^{-1}$, $B_-B_+^{-1}$, $(I - B_-B_+^{-1})^{-1}$, and $(I - (B_-B_+^{-1})^2)^{-1}$ are read into permanent storage.

The basic shielding calculations are performed in step four. Various matrix-vector operations are needed for this step. Infinite reflection and source backing conditions are used as options. Transmitted and reflected fluxes for a plane source can be obtained by the

---

[1]The IMSL (International Mathematical and Statistical Libraries, Inc.) Library contains 245 subroutines compatible with FORTRAN IV.

multiplications of $T(x)\underline{S}$ and $R(x)T(x)\underline{S}$, respectively. For point source problems, the derivative and integrations of T(x) are needed from Eqs. (44) and (45). Based on Eqs. (29), (40), and (41), the distributions in the forward and backward directions are obtained.

A major computational advantage for this method is that the results from the first three steps are common to problems for different spatial configurations. The bulk of the computing time for a single problem goes into evaluating the matrices $B_{\pm}$ and $C_{\pm}$. These are specific for each material but do not depend on the shielding thickness. The H, T, and R matrices for a shield are characteristic only of the material and the thickness of the shield, and do not depend on the remainder of the configuration. Thus intermediate results can be stored on tape and never need to be recomputed.

A basic problem with the input data is to determine how many terms are needed for the angular expansion. The number required depends not only on the type of angular expansion functions but also on the width of the energy groups. Legendre polynomials in angular expansions and GAM-II energy groups were used for the present work.

In order to determine the required angular terms, fast neutron shielding by sodium was selected as an example for the investigation. Group 19 in Table 2 was chosen to be the source group and, due to the downscatter property, neutrons were slowed down to lower energy groups. After group 23, the energy was "cut-off." Transmitted energy spectra for sodium for a variety of thicknesses at various angles using different angular terms were calculated and the results were plotted in Figs. 2, 3, and 4.

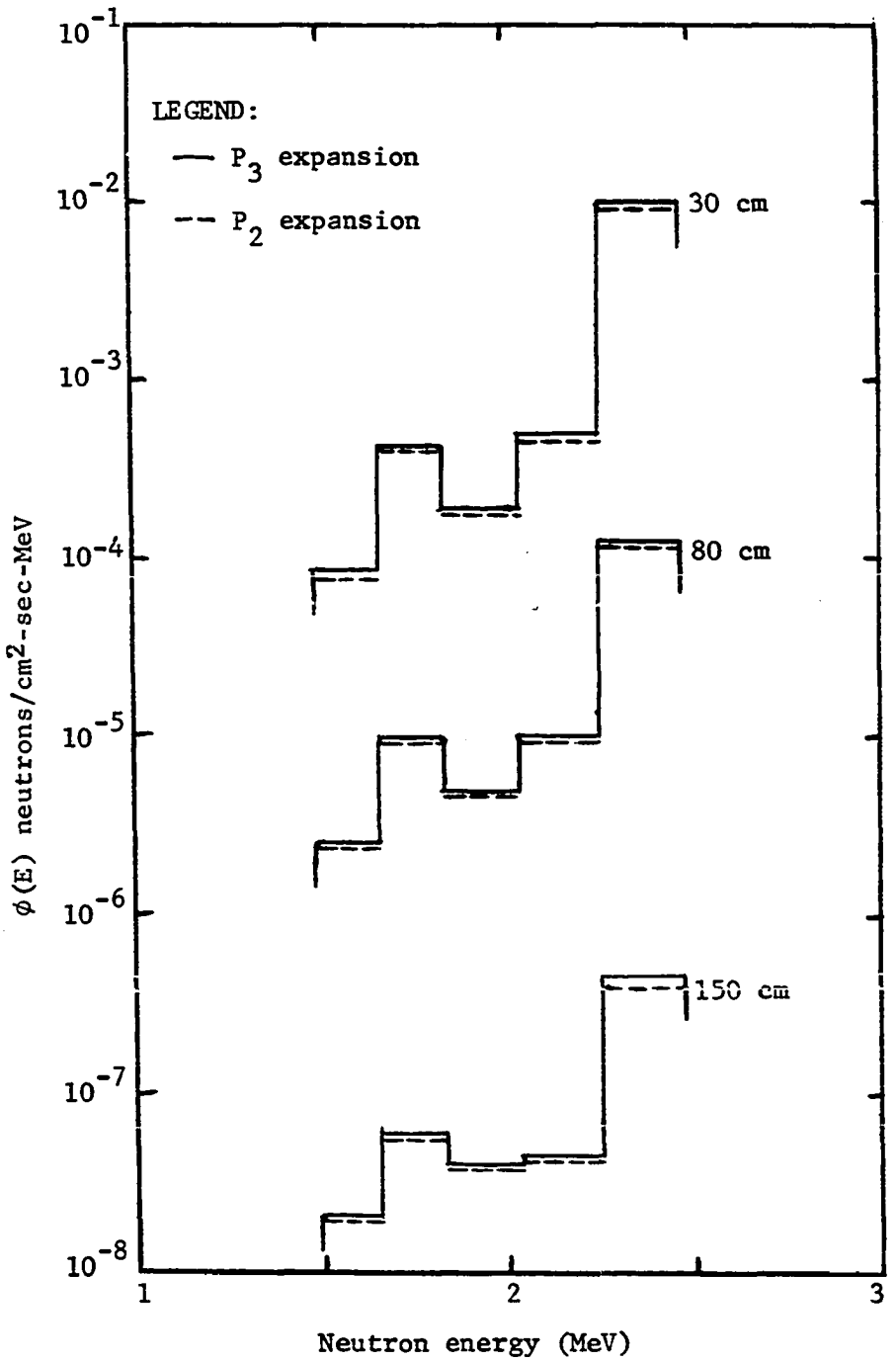


Fig. 2. Transmitted neutron spectra in sodium at various distances from a plane isotropic source with energy from 2.23 to 2.47 MeV

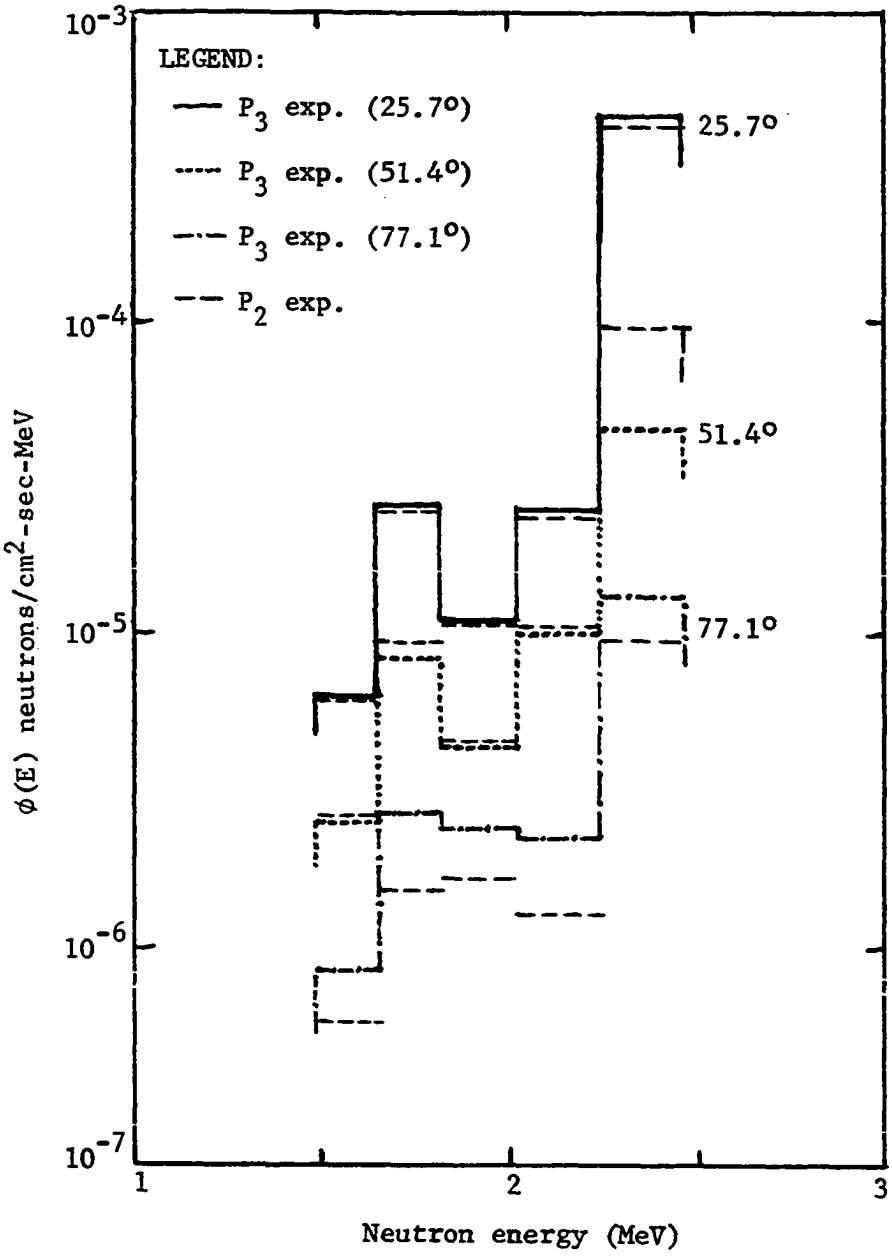


Fig. 3. Transmitted neutron energy spectra beyond 80 cm sodium at various angles from a plane isotropic source with energy group from 2.23 to 2.47 MeV

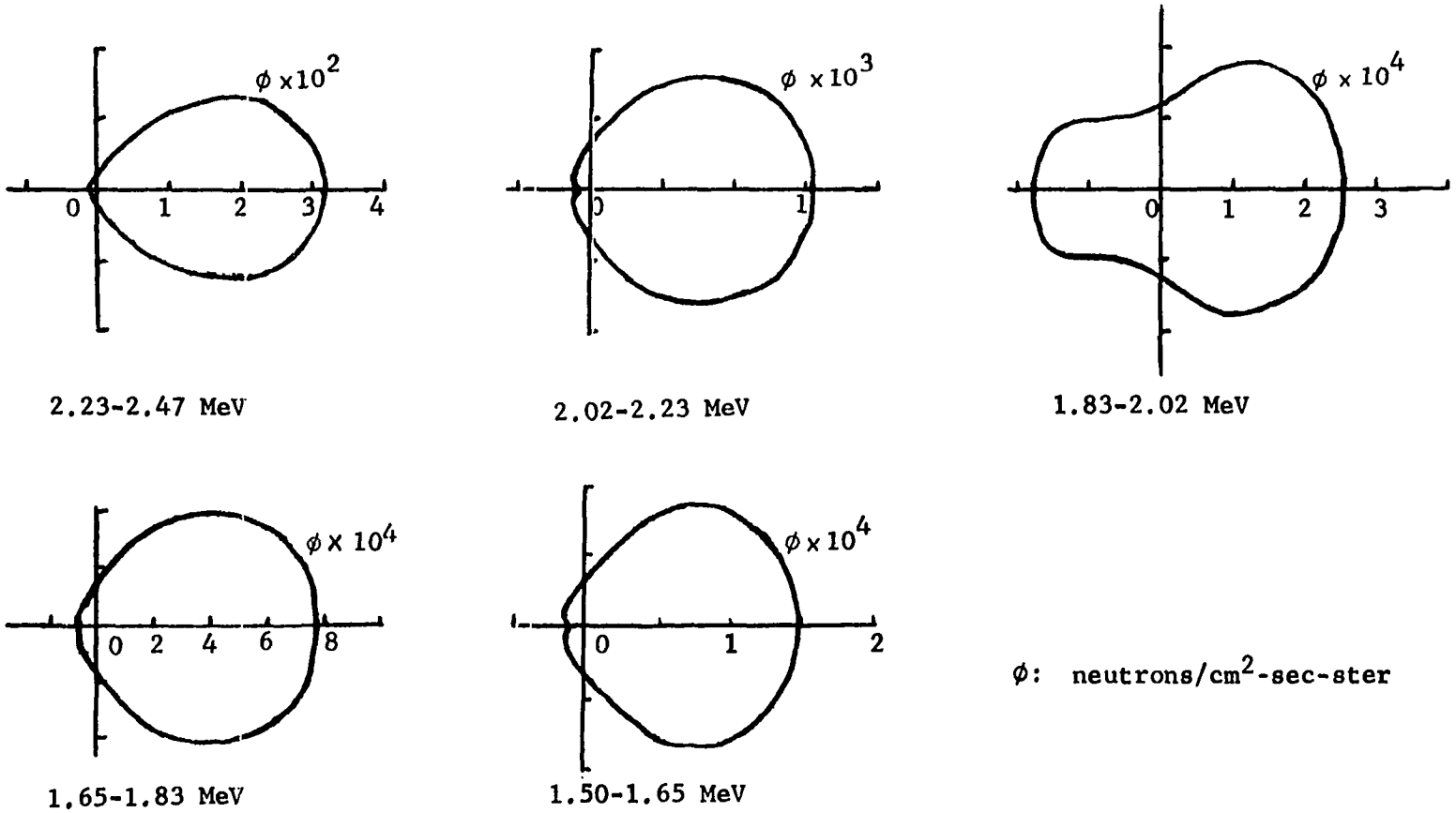


Fig. 4. Angular flux distributions due to a 2.23 to 2.47 MeV plane isotropic source incident upon 30 cm sodium

Four different angular terms were used in the primary calculation. In Fig. 2, no significant difference could be observed by using different angular terms. The solutions of $P_4$ and $P_5$ approximations fell between those of the $P_2$ and $P_3$ approximations. In Table 3 is shown the numerical results of transmitted fluxes through 80 cm of sodium by using four different angular expansion terms. An asymptotic solution can be found by taking an infinite number of angular terms. However, disagreements for measured angles larger than 50° by taking different angular terms are observed, as shown in Fig. 3. Therefore, more angular terms are required for spectra at large angles from the normal.

Table 3. Transmission through 80 cm of sodium, in units of neutrons/cm$^2$-sec-MeV. Isotropically incident flux normalized to 1 neutron/cm$^2$-sec

| Energy group | Angular expansion | | | |
|---|---|---|---|---|
| | $P_2$ | $P_3$ | $P_4$ | $P_5$ |
| 19 | $1.179 \times 10^{-4}$ | $1.256 \times 10^{-4}$ | $1.208 \times 10^{-4}$ | $1.238 \times 10^{-4}$ |
| 20 | $9.747 \times 10^{-6}$ | $1.025 \times 10^{-5}$ | $1.000 \times 10^{-5}$ | $1.020 \times 10^{-5}$ |
| 21 | $4.945 \times 10^{-6}$ | $5.131 \times 10^{-6}$ | $5.044 \times 10^{-6}$ | $5.117 \times 10^{-6}$ |
| 22 | $9.609 \times 10^{-6}$ | $1.006 \times 10^{-5}$ | $9.843 \times 10^{-6}$ | $1.002 \times 10^{-5}$ |
| 23 | $2.590 \times 10^{-6}$ | $2.708 \times 10^{-6}$ | $2.658 \times 10^{-6}$ | $2.704 \times 10^{-6}$ |

If the asymptotic solution is assumed to be the "exact" solution, then the error due to $P_3$ expansions can be estimated by calculating the differences between the solutions of $P_3$ and $P_4$ expansions. In Table 3, the differences between the $P_3$ and $P_4$ expansions are 4% for the source group and $< 3\%$ for the rest of the groups. Therefore a 4% error due to a $P_3$

approximation can be expected. This value, however, is an overestimated value, since most of the transport calculations using $P_3$ approximations for the elastic scattering angular distributions gave reasonable results [18]. Thus $P_3$ expansions were chosen for later work.

# V. RESULTS AND DISCUSSION

The transfer matrix method was employed to compute the angular energy distributions of fast neutrons from a monoenergetic source and from a fission spectrum. Comparisons between the calculated and experimental spectral distributions were made and used to evaluate the validity of the calculation method, to establish the limits of its application, and to check average group cross sections used in the calculation.

It is evident that the angular energy distributions depend on the spectrum and geometry of the neutron source, the physical properties of the medium, the boundary conditions, etc. In order to make the comparison, specifications of these conditions in the calculation and the experiment are required.

The angular energy spectra beyond the iron layer due to a 3.01-3.32 MeV point isotropic source were calculated by the transfer matrix method and the results were plotted in Figs. 5 through 8. The experimental results were taken from Ref. [15]. In the experiment a neutron source based on the D(D, n)$He^3$ reaction was used. The experimental setup was centered at a medium-water interface. This reaction provides a point isotropic source, which may be regarded as monoenergetic. The experimental data were obtained by the integrated recoil-nuclei method (with a single crystal scintillation spectrometer). This experiment often has low accuracy (10-40%), because of the method used for transforming the amplitude distributions to the required spectra. Hence, the comparison of calculated and experimental data cannot be considered in an exact sense. The experimental and calculated

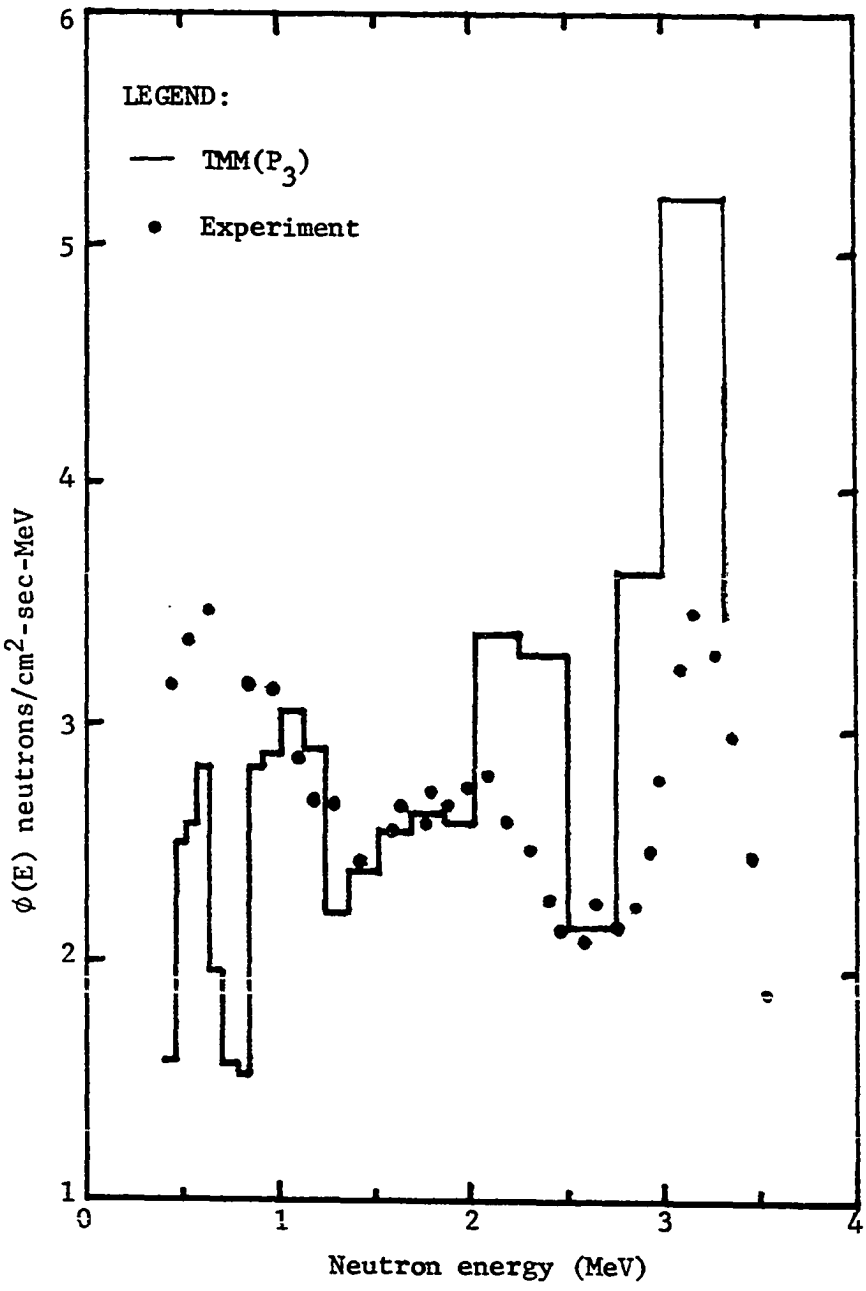


Fig. 5. Neutron spectra at 20° beyond 16 cm of iron from a point monoenergetic source

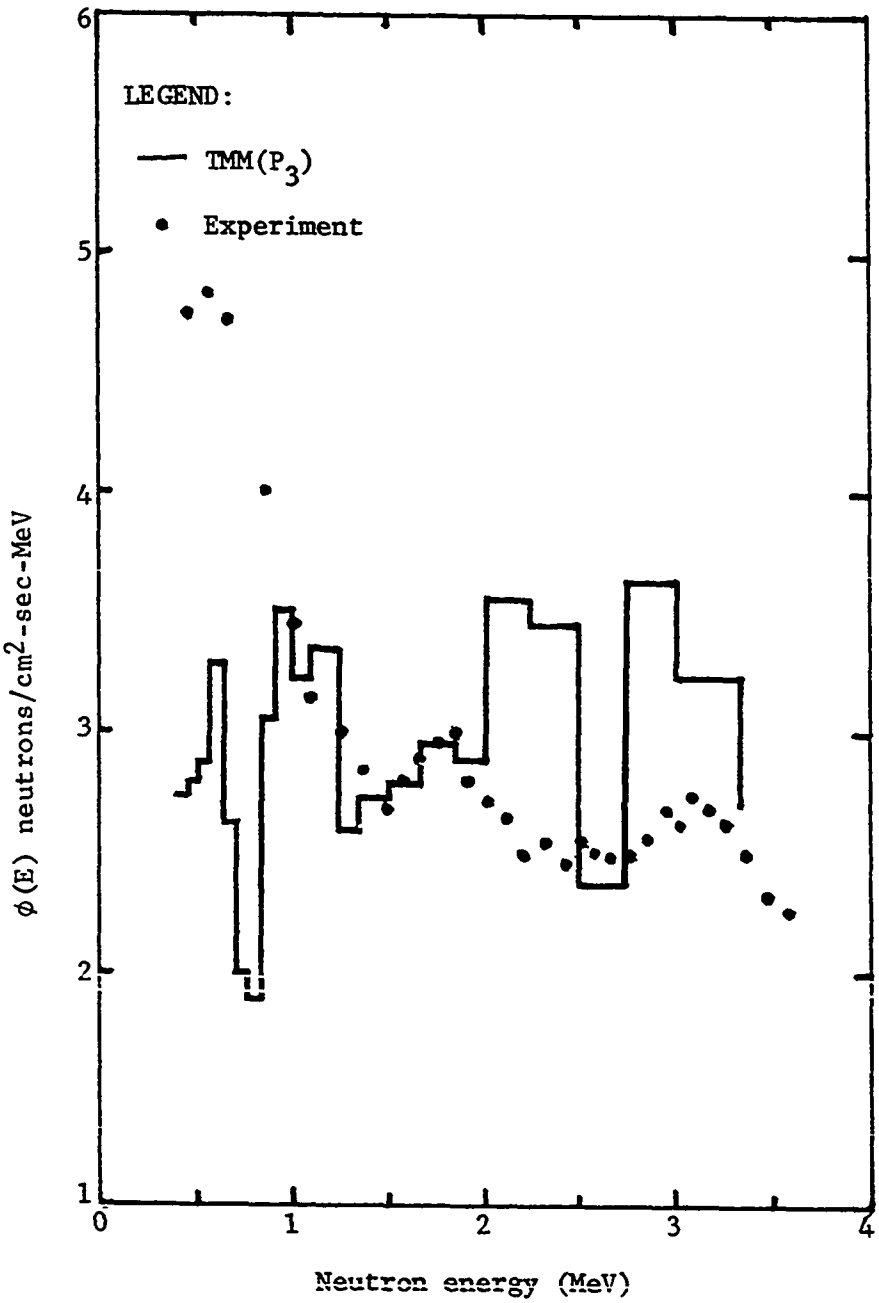


Fig. 6. Neutron spectra at 40° beyond 16 cm of iron from a point monoenergetic source

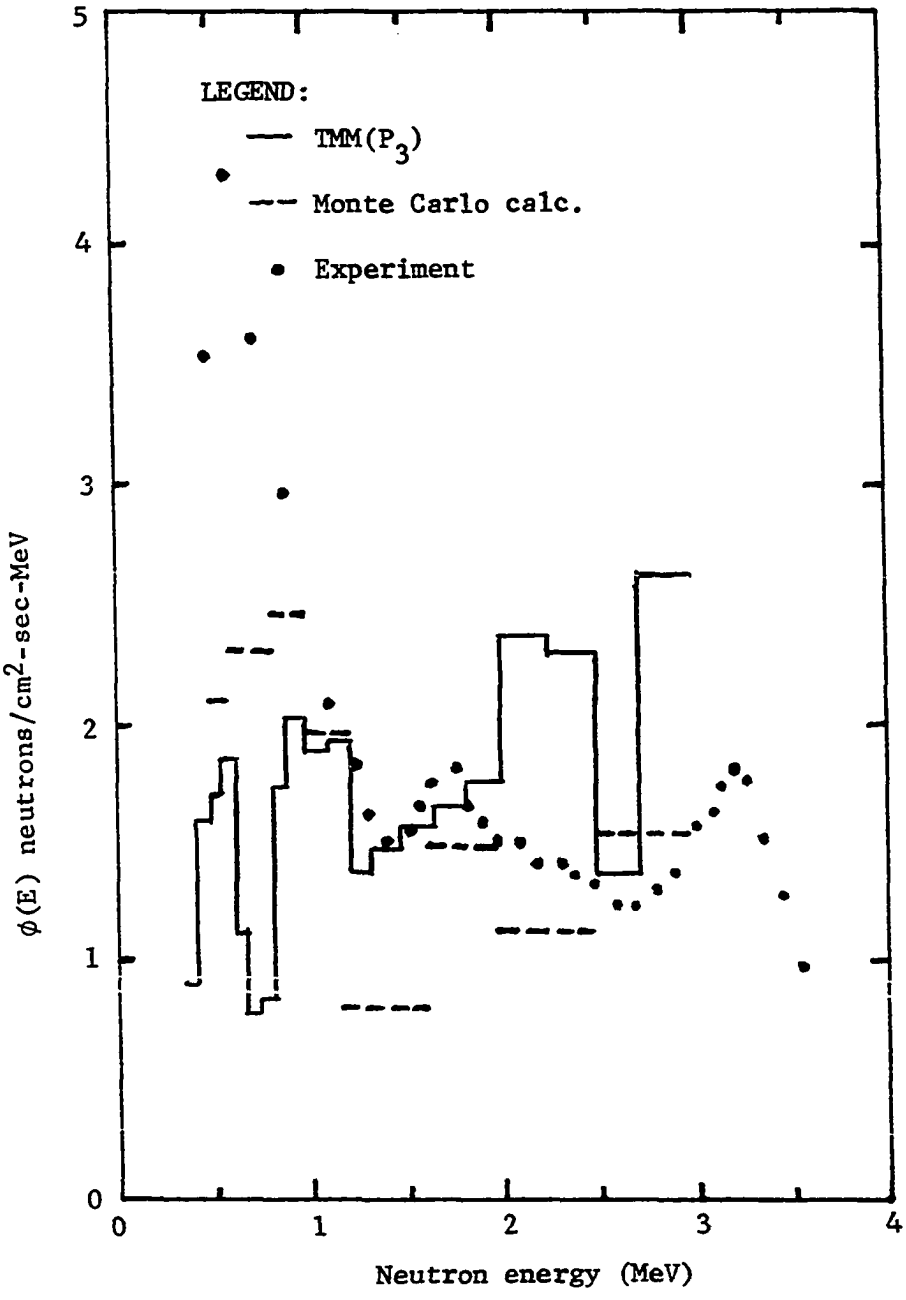


Fig. 7. Neutron spectra on the centerline beyond 10.3 cm of iron

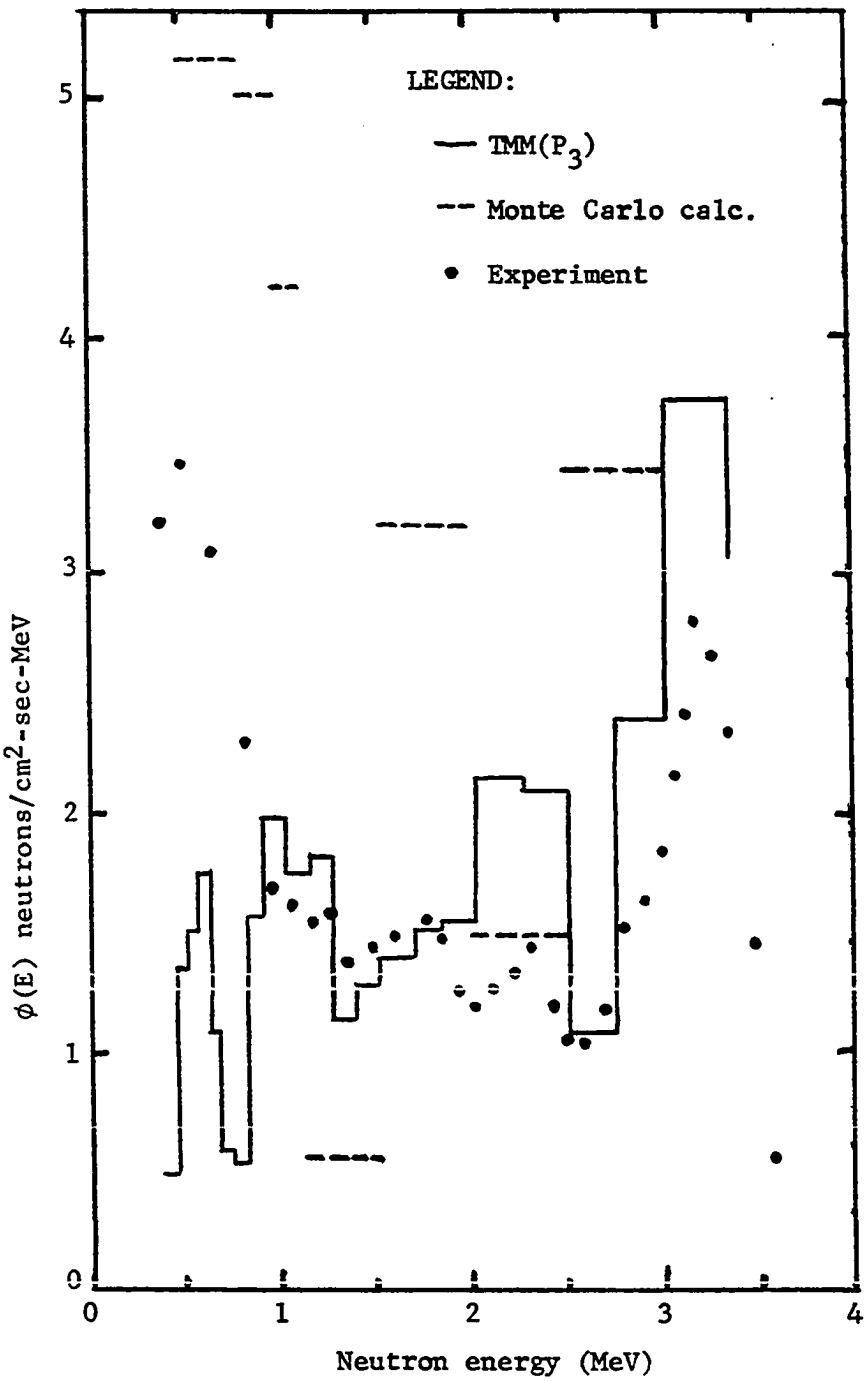


Fig. 8. Neutron spectra on the centerline beyond 16 cm of iron

angular energy spectra were normalized to the same level in the region 1.50 to 1.65 MeV.

In Figs. 5 and 6, comparisons are shown between the calculated and experimental angular energy spectra at angles of 20 and 40° from the normal behind 16 cm of iron. The elastic scattering peak appears at energies near the source energy. A sharp peak at the source group is observed in the calculated spectrum. This is due to narrow energy groups and deficient angular terms used in the transfer matrix calculation. Both experimental and calculated spectra show the minima in the energy ranges 2.47 to 2.73 MeV and 1.22 to 1.35 MeV, which correspond to the resonances in the iron cross section as shown in Fig. 9. The calculated spectra were obtained under the infinite medium assumption, while the experimental data were taken using a water-medium boundary. The reflection from the water gave a pronounced peak at energies below 1 MeV. In the calculated spectra, there are explicit peaks and valleys as compared with values obtained in the experiment. Part of the error is due to the use of a group processing code with $P_3$ and $P_0$ truncations of the angular distributions arising from elastic and inelastic scattering, respectively. However, the overall agreement is good at 20° but inadequate at 40°. The discrepancies which occurred at 40° are due to the deficient expansion terms used in the angular fluxes.

In Figs. 7 and 8 are given the experimental energy spectra after penetrating iron layers (10.3 and 16 cm). Results are also given in Figs. 7 and 8 for transfer matrix calculations of the energy distributions in iron with an isotropic point source. Monte Carlo calculations [9]

in iron from a plane, monodirectional source of 3 MeV neutrons is also shown. The experimental source spectrum and the monoenergetic neutron source used for transfer matrix calculations are shown in Fig. 10. Comparison of the spectra indicates an overestimate by the transfer matrix method in the energy region 2 to 2.5 MeV still exists.

The angular energy distributions through iron and sodium from a fission source were calculated. These materials were chosen because of their practical applications in the Liquid Metal Fast Breeder Reactor (LMFBR). A 27-energy-group structure is used to cover the neutron energies from 1 MeV to 15 MeV. In order to avoid very large matrix calculations, a $P_2$ expansion in angular distributions was chosen for the rest of the work. From Table 3, an underestimate is predicted for the calculation using $P_2$ expansions.

In Fig. 11 is shown the transmitted neutron spectra through iron at various distances in the semi-infinite medium from an infinite plane isotropic fission source. The increase of the flux with energies above 7 MeV in the 65 cm of iron is due to the infinite reflections of the material. The reflected neutron spectra of the iron at the corresponding distances are also shown in Fig. 12. Based on Fig. 11, the fast neutron relaxation length in iron is about 3.7 cm which is lower than 6 cm as given in Ref. [11].

In Figs. 13, 14, 15, and 16 are shown the experimental and calculated neutron spectra through iron at various angles and distances from a fission source. The calculated and experimental results are normalized to the same level at 3 MeV for 30.48 cm of iron measured on the normal. The experimental results and neutron source spectra in Figs. 13 through 17

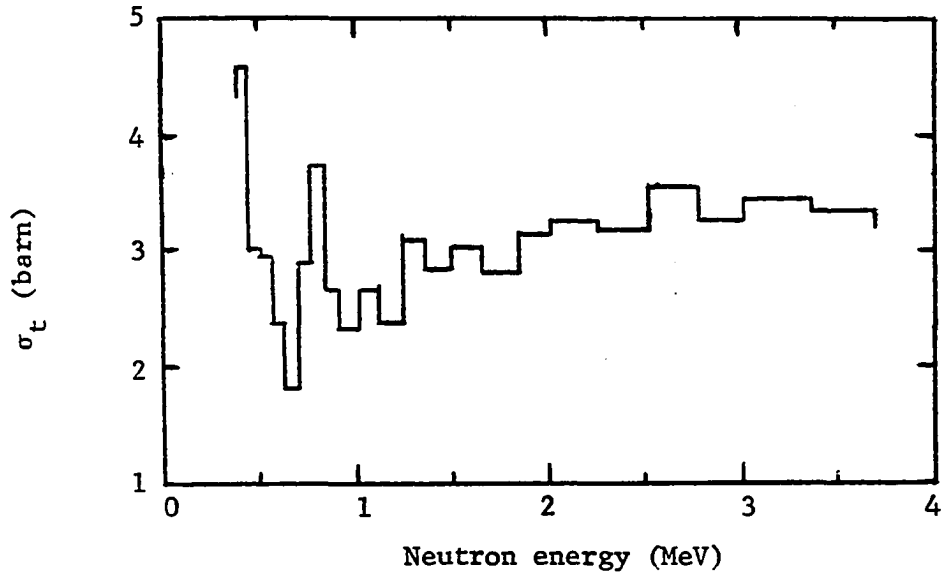


Fig. 9. Total neutron cross section of iron from DLC-2/100G (MAT 1180)

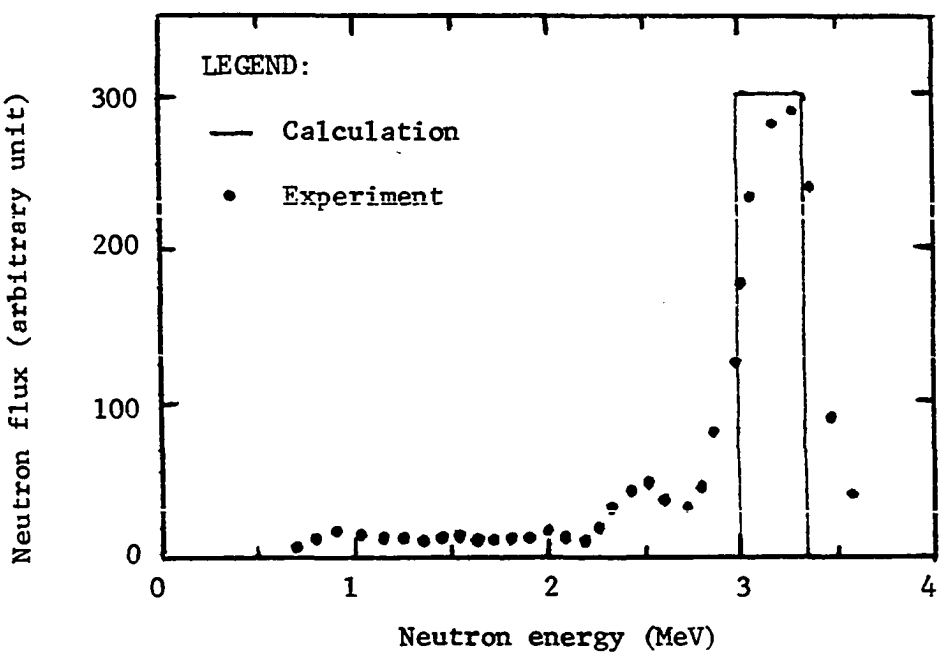


Fig. 10. Monoenergetic neutron source used in the calculation and experiment

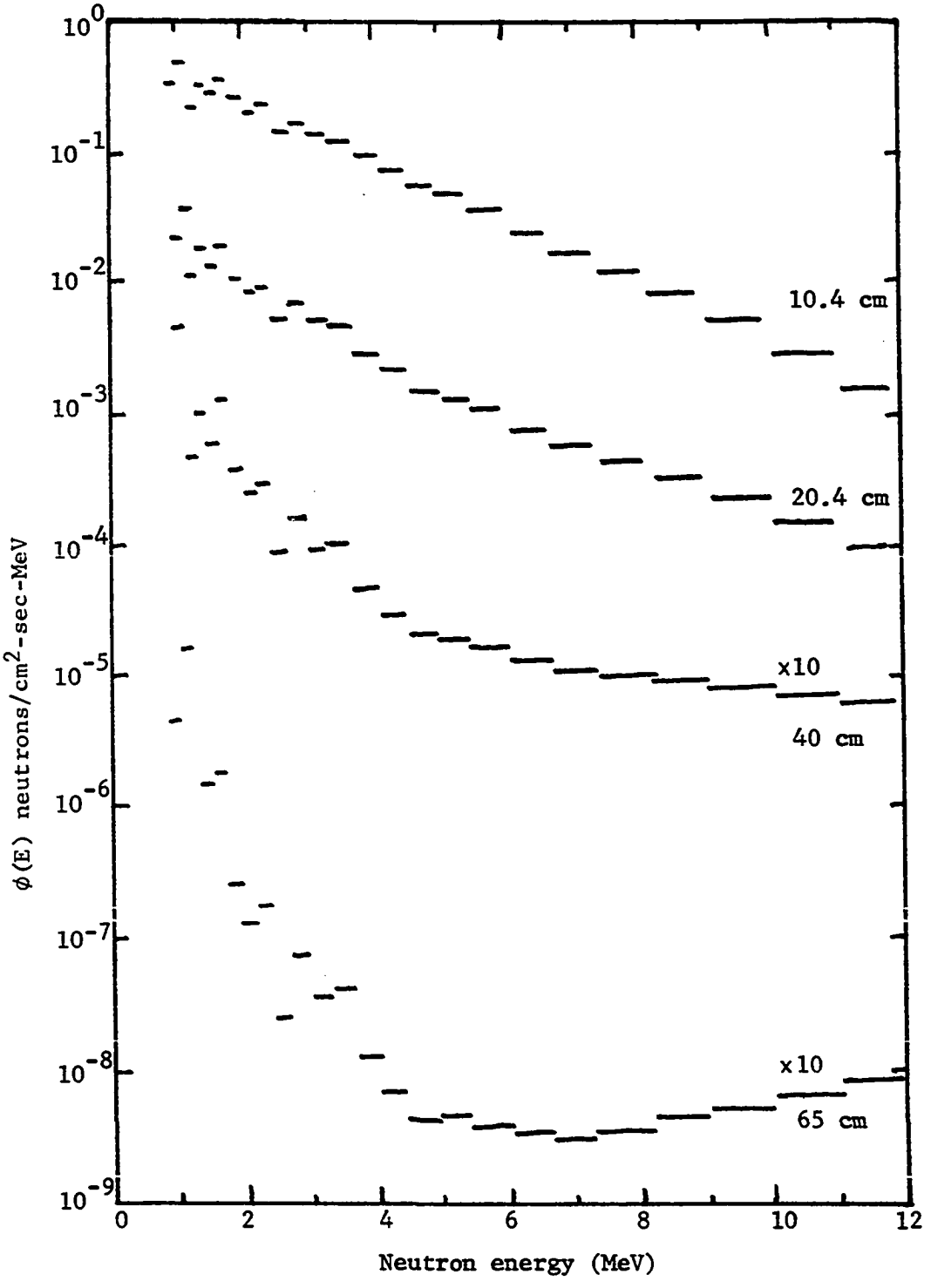


Fig. 11. Neutron spectra at various distances in iron from a plane isotropic fission source

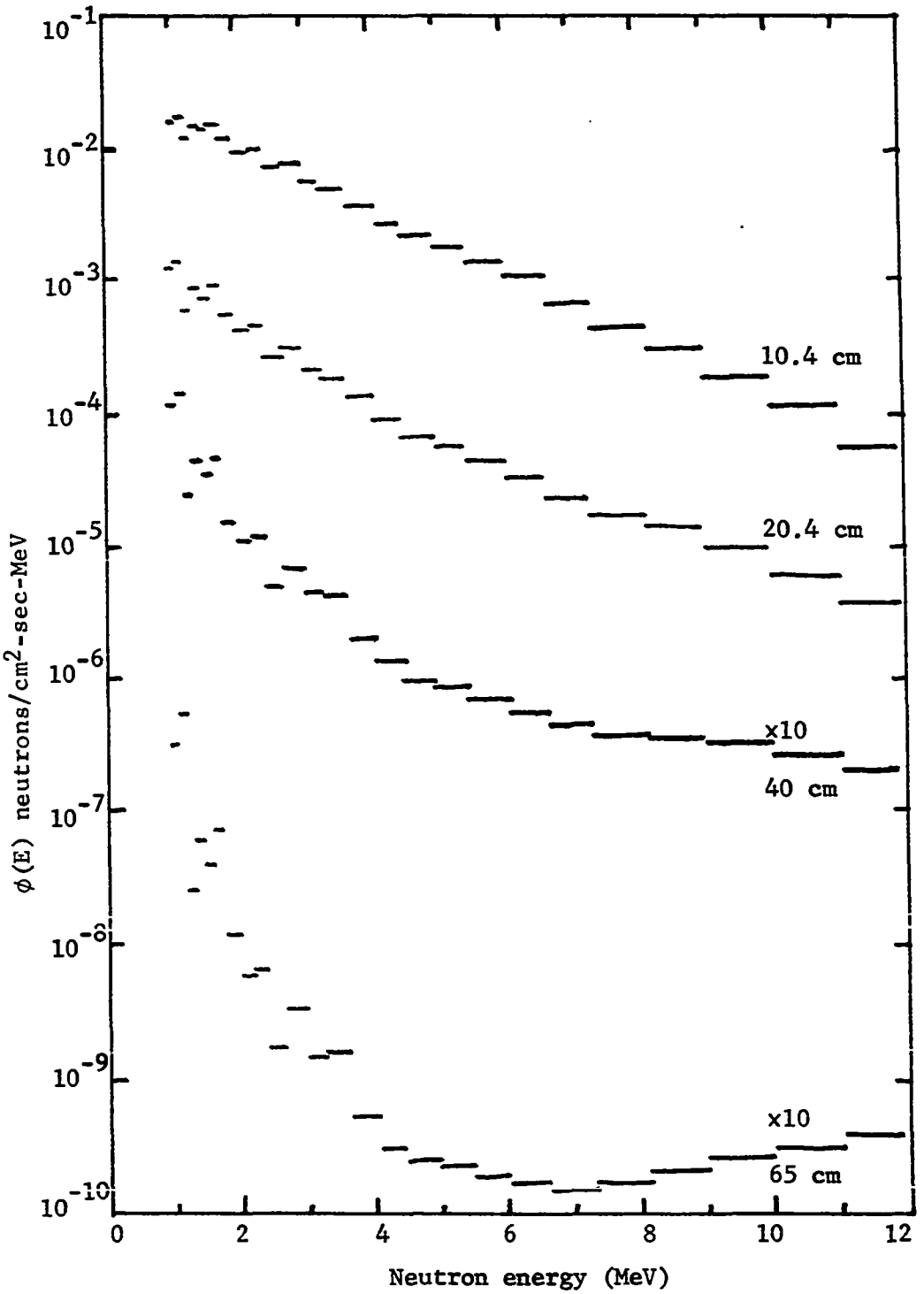


Fig. 12. Reflected neutron spectra at various distances in iron from a plane isotropic fission source

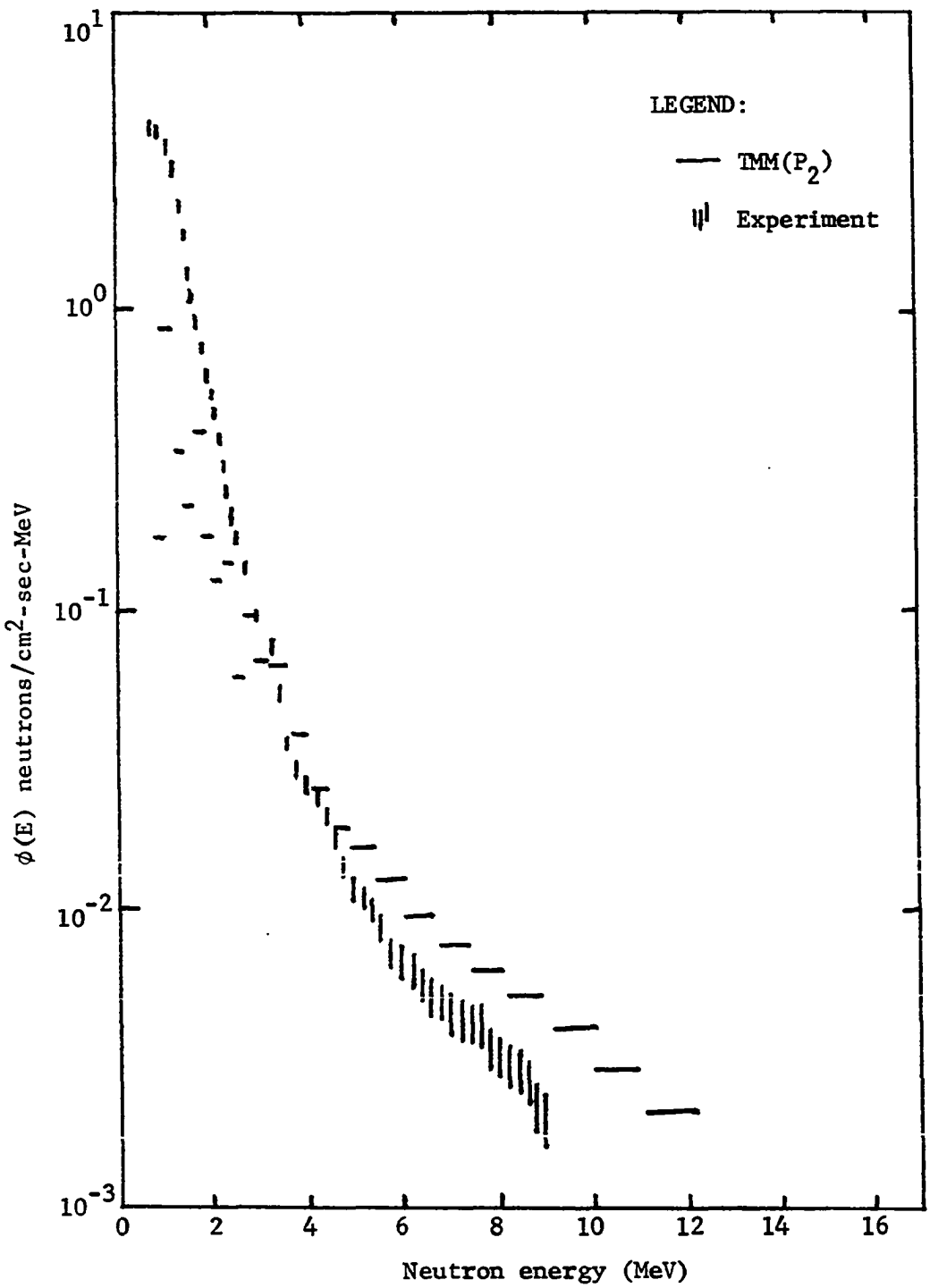


Fig. 13. Neutron spectra on the centerline beyond 30.48 cm of iron from a point fission source

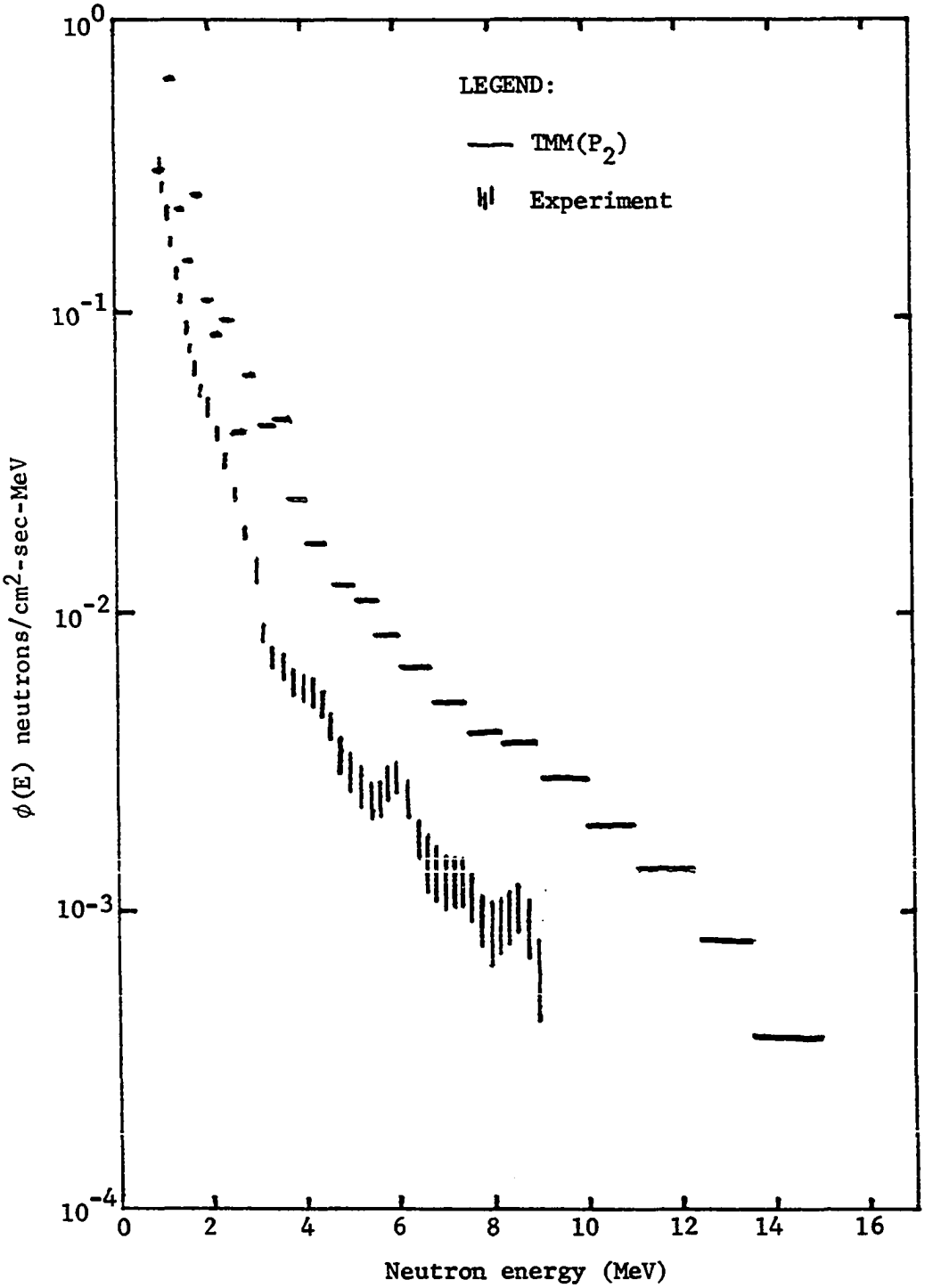


Fig. 14. Neutron spectra at 15° off the centerline beyond 30.48 cm of iron from a point fission source

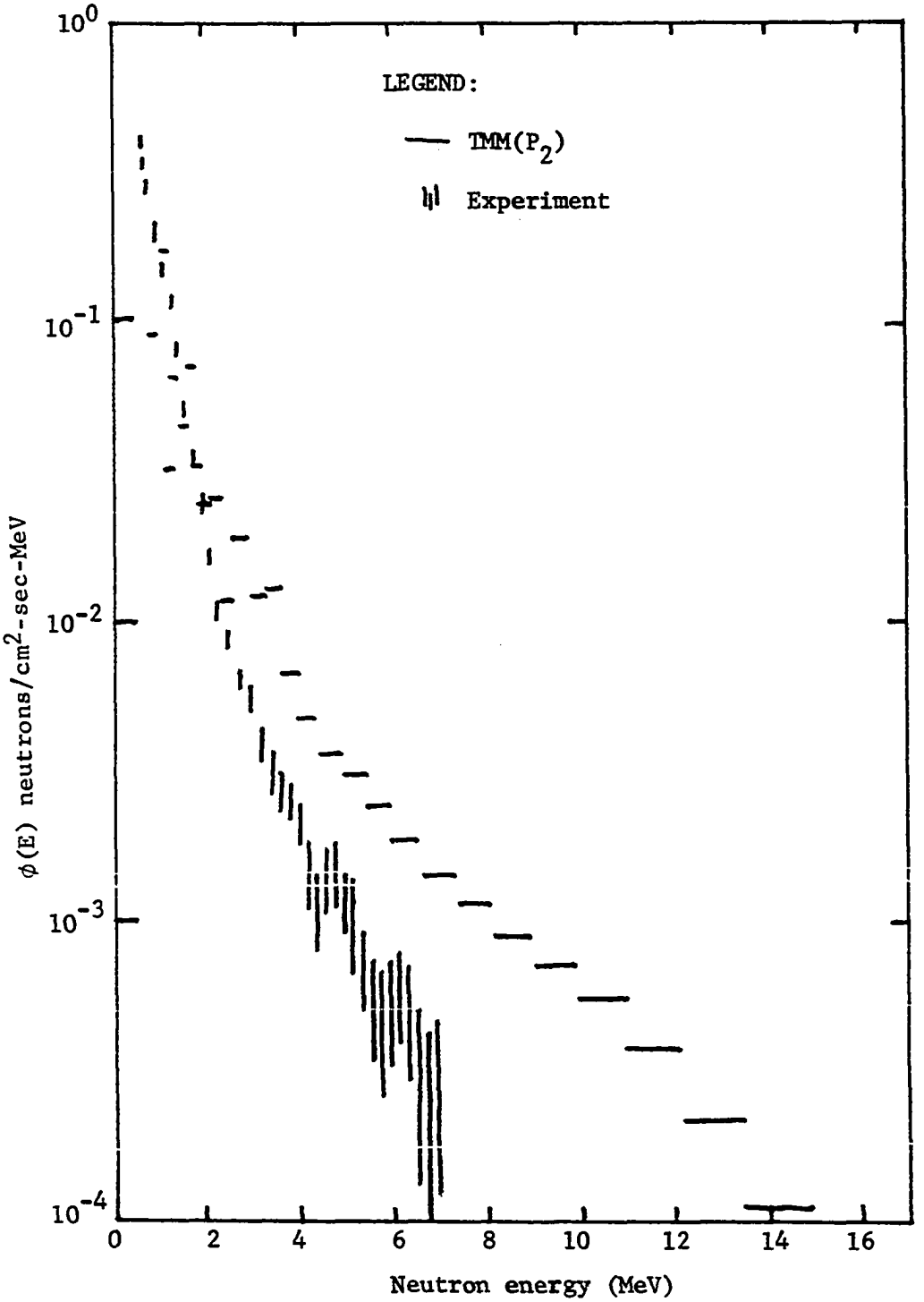


Fig. 15. Neutron spectra at 45° off the centerline beyond 30.48 cm of iron from a point fission source

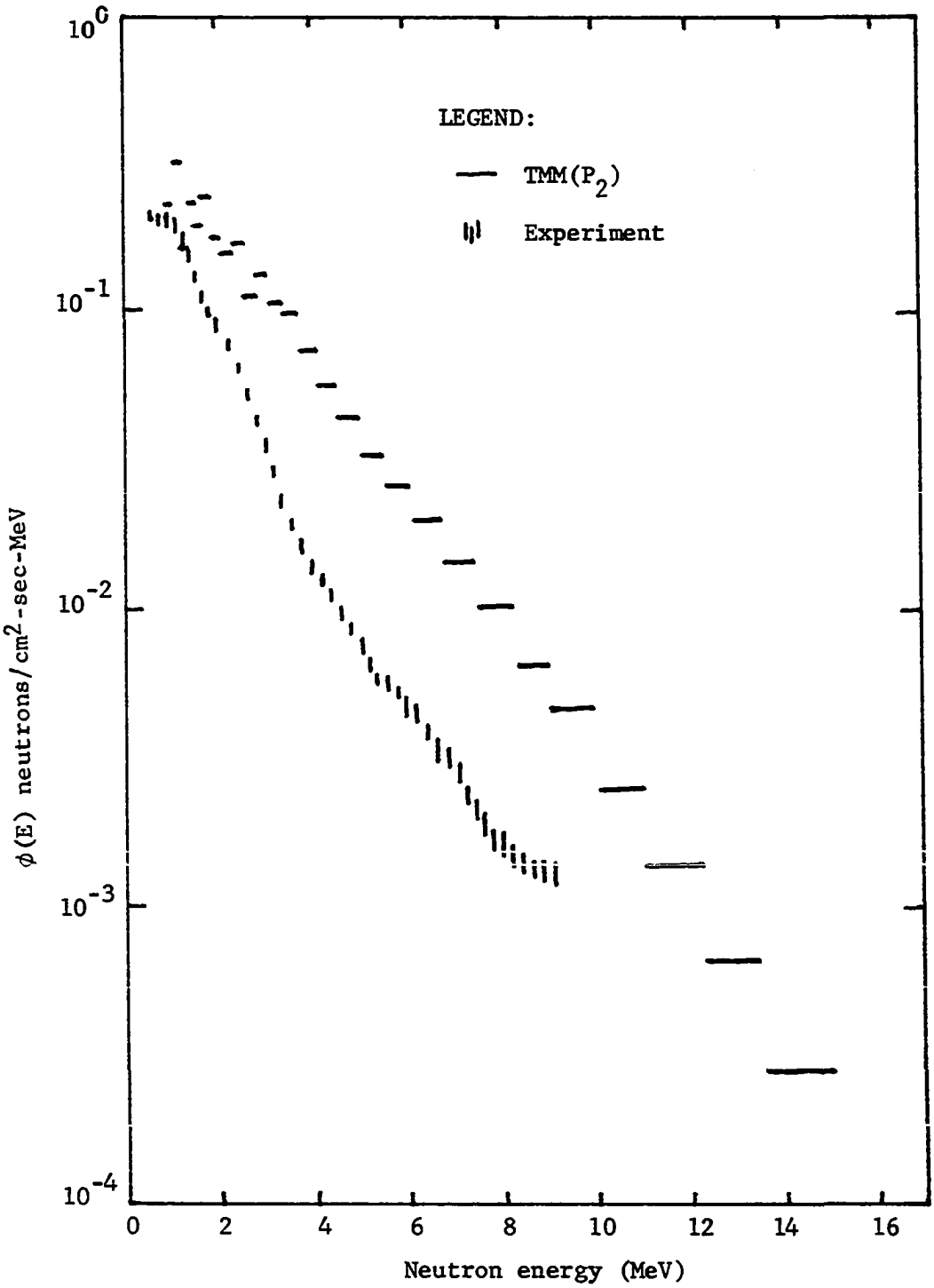


Fig. 16. Neutron spectra on the centerline beyond 15.24 cm of iron from a point fission source

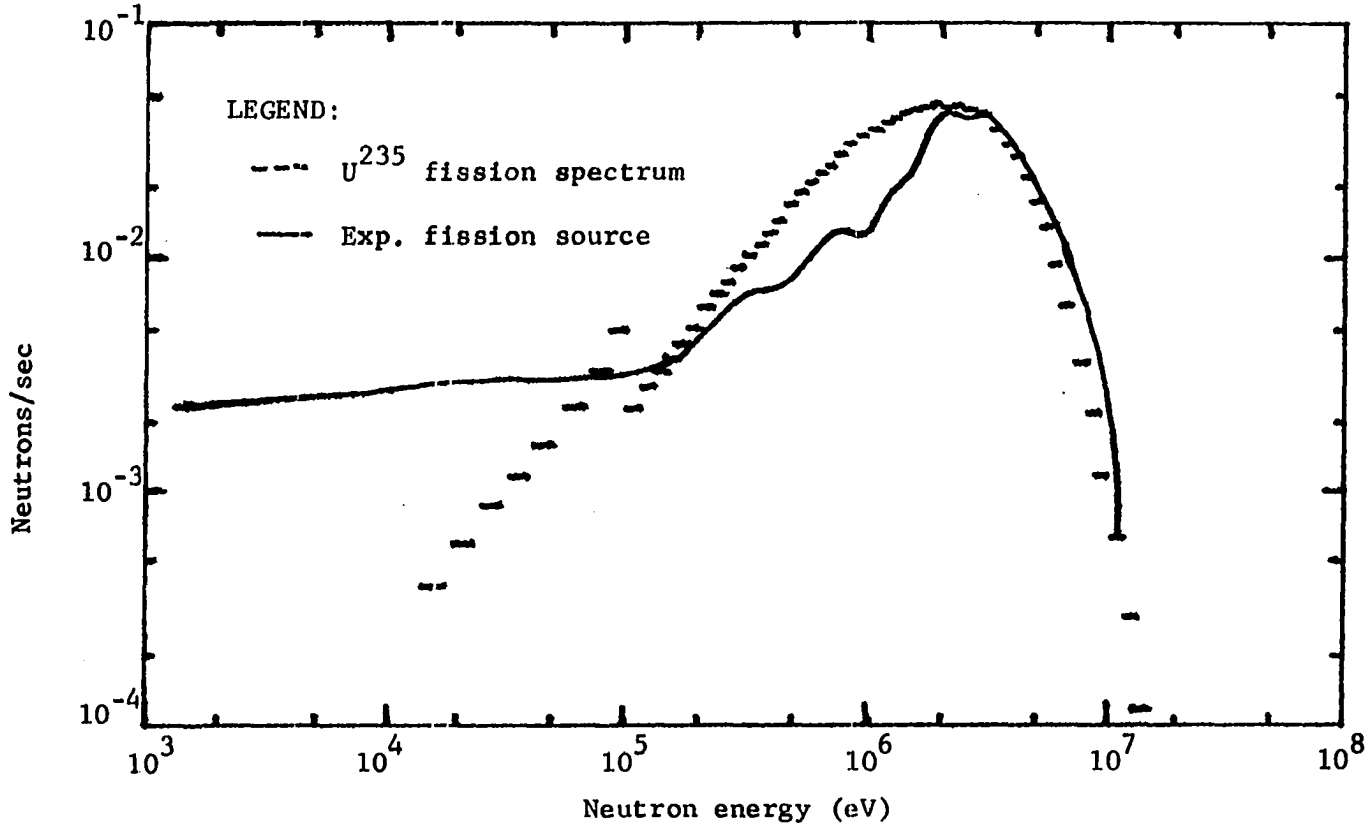


Fig. 17. U-235 fission spectrum and experimental fission source

are obtained from Ref. [18]. The collimated neutron beam from the Tower Shielding Facility (TSF-II), which was used as a neutron source for the experiment, has been shown to be a point anisotropic source. The fission spectrum used in the transfer matrix calculations is taken from Ref. [13] as shown in Fig. 17. The source geometry was chosen to be point isotropic.

In the calculated results it is shown that for a 30.48 cm iron slab there is a slight overestimate above 5 MeV and a slight underestimate below 2 MeV at the $0^{o}$, about a 3.5 factor overestimate above 3 MeV at $15^{o}$ off the normal, and 2.5 factor overestimate above 4 MeV at $45^{o}$ off the normal. The discrepancy in the off-normal cases is due to insufficient angular terms used in the calculation. An overestimate is observed in 15.24 cm of iron. The experimental results include multiple reflections between the iron slab and the reactor collimator, the iron collar and water shield surrounding the collimator. These effects were not added to the calculated results which were obtained using a vacuum boundary at both front and back of the slab. The experimental slabs were not pure iron (98% iron, 1.5% carbon, 0.5% manganese) and the anisotropic source used for the experiment are other possible reasons for errors. Slightly different fission sources were used for the calculation and experiment as shown in Fig. 17. This effect could be also added to the disagreement.

In Fig. 18 is shown the energy distributions of 30 cm of sodium at the angles of 20, 40, and $70^{o}$ from an infinite plane isotropic fission source. It will be noted that the shape of the energy spectrum does not change too much from one angle to another. Sodium

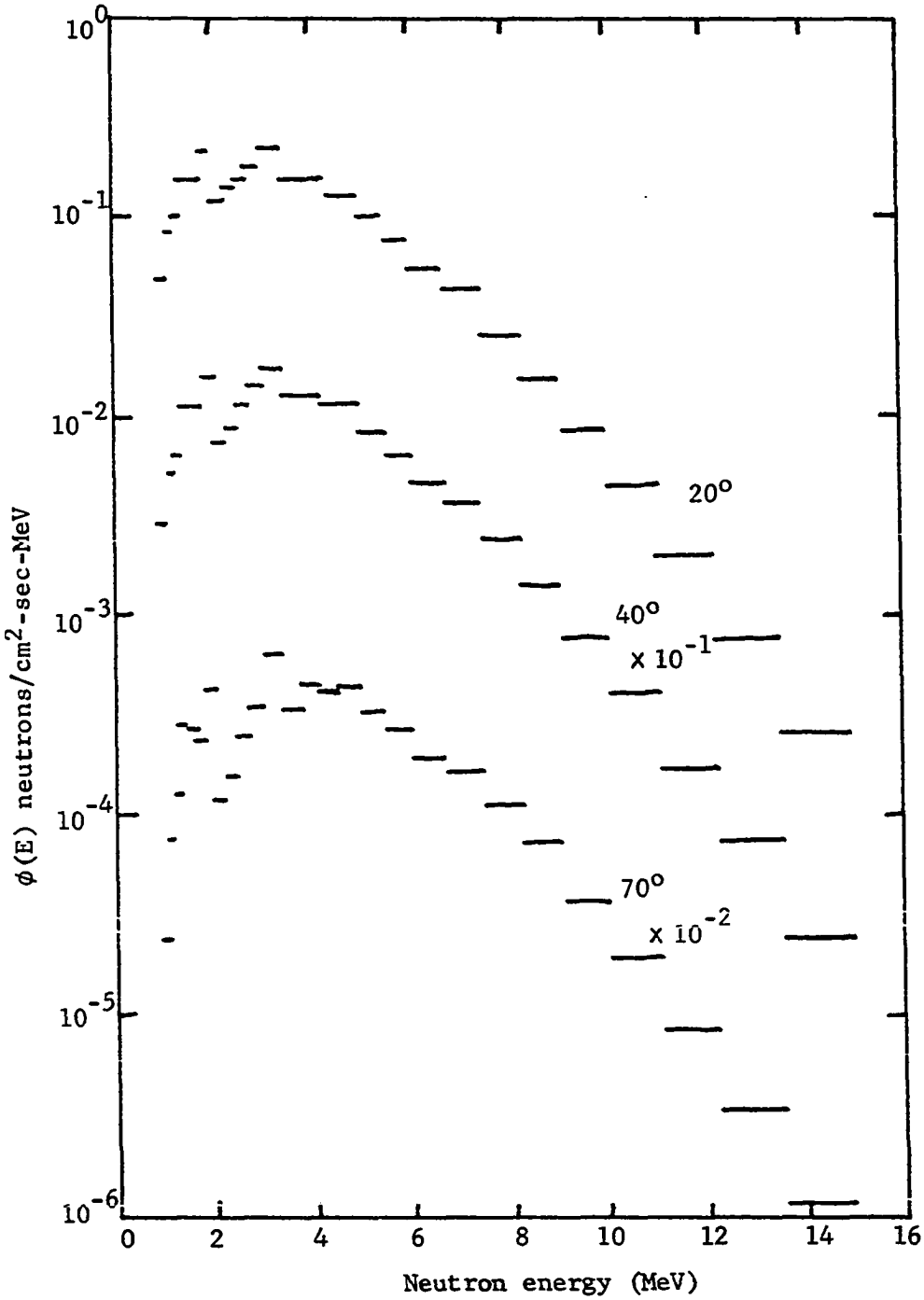


Fig. 18. Neutron spectra in 30 cm of sodium at various angles from a plane isotropic fission source

energy spectra at various distances from a point isotropic fission source are also given in Fig. 19. A tendency of spectrum hardening with increasing thickness can be observed.

In Fig. 20 is given a comparison of calculated and experimental energy spectra through 152.4 cm of sodium at the normal due to a point isotropic source. The experiment was performed in the Tower Shielding Facility. From the energy spectrum obtained in the experiment [21], one can see three valleys at 2 MeV, 3.5 MeV, and 5.5 MeV. These values correspond to 2 MeV, 3.5 MeV, and 6 MeV in the calculated spectrum. However, a significant disagreement is found below 3 MeV. Analysis of the data from the transfer matrix calculation shows that the fast neutron relaxation length in sodium is 18.8 cm. The reported experimental value is about 24 cm [27].

In general, the shapes of the calculated spectra of iron and sodium are similar to those of the experimental results. This result indicates that the average group cross sections used for the calculation are overall correct. However, the average total cross section of the iron in the region 1 to 2.5 MeV is too high in the DLC-2/100G evaluations. This conclusion is in agreement with the results given in Ref. [18].

For both calculated iron and sodium spectra, there are smooth curves above 4 MeV while undulations occurred below 2.5 MeV. For energies below 2.5 MeV, fine energy grouping was used. If the groups are narrow, each eigendistribution will be sharply peaked in angle in its group and many angular terms must be used to represent the peak

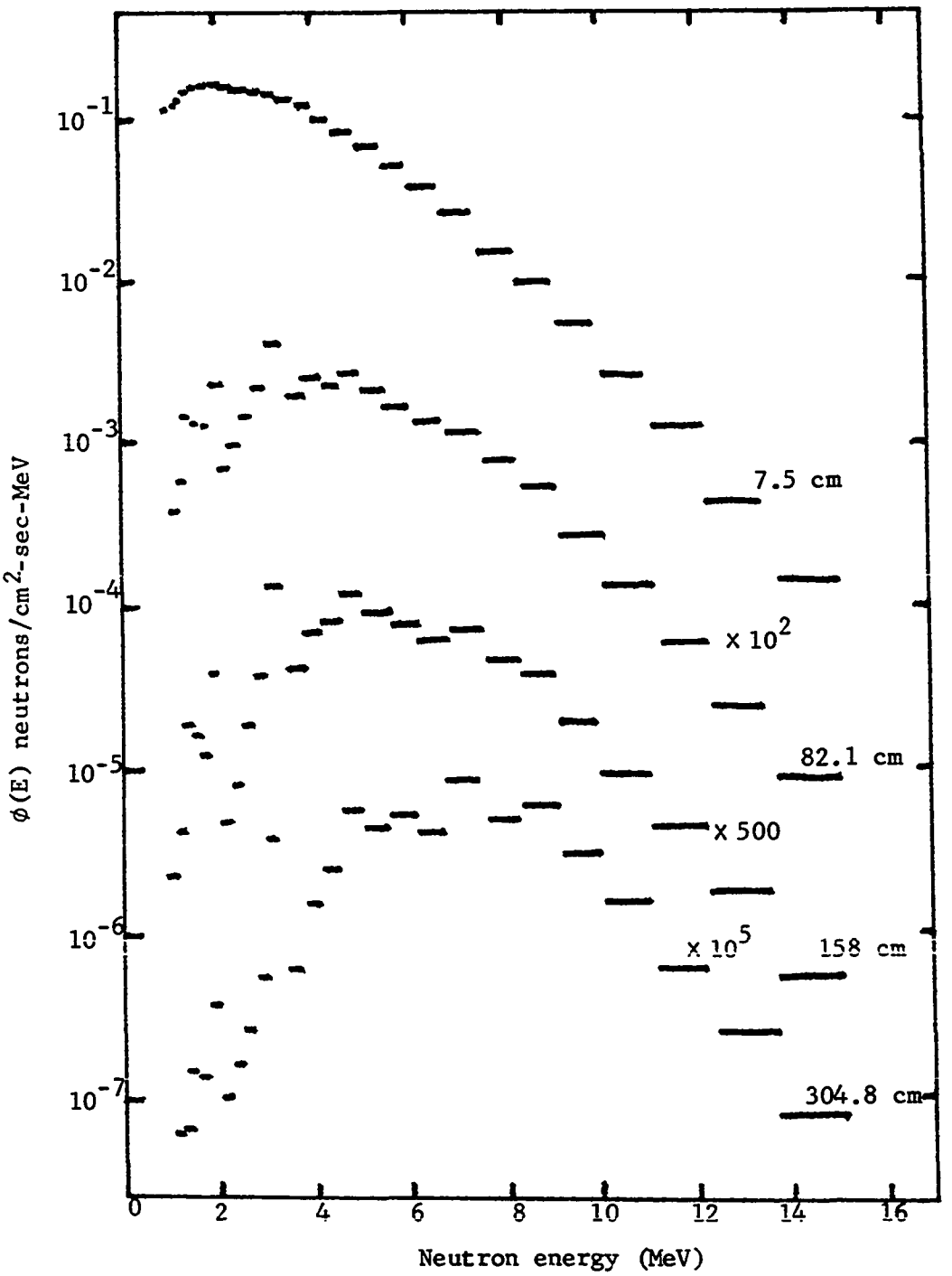


Fig. 19. Neutron spectra in sodium at various distances from a point isotropic fission source

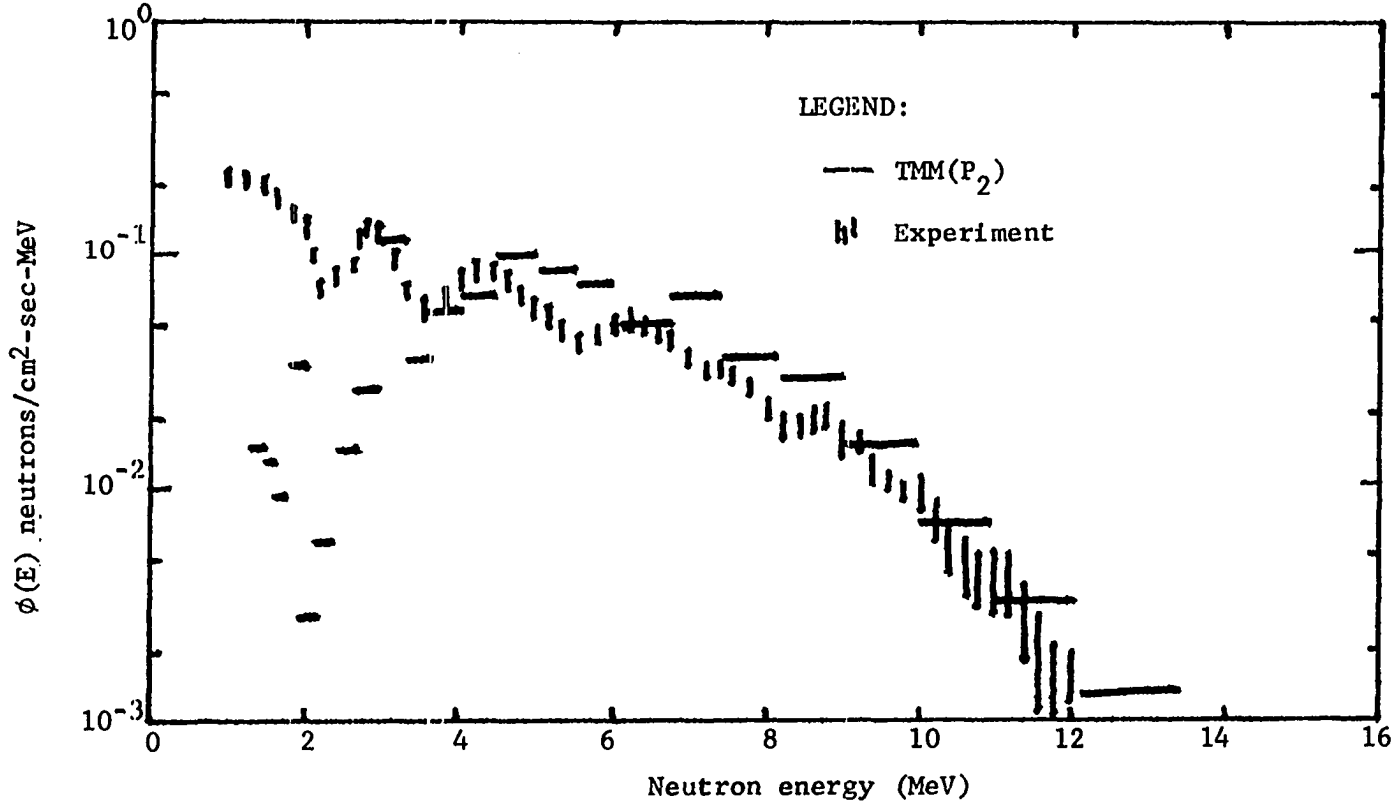


Fig. 20. Neutron spectra on the centerline beyond 152.4 cm of sodium from a point fission source

adequately. Since coarse energy groupings were used for energies above 4 MeV, fewer angular terms were required.

The shortening of the relaxation lengths of sodium and iron leads to underestimation of the result. This disagreement can be improved by taking more angular terms for the angular distributions. Aronson and Yarmush [3] suggested that seven terms (through $P_6$) in a double-$P_n$ expansion for the energy grouping should suffice for a good representation of total flux and current out to 15 mean free paths.

The transmission from a point isotropic fission source through the sodium-iron layers was also investigated and the results were plotted in Figs. 21 and 22.

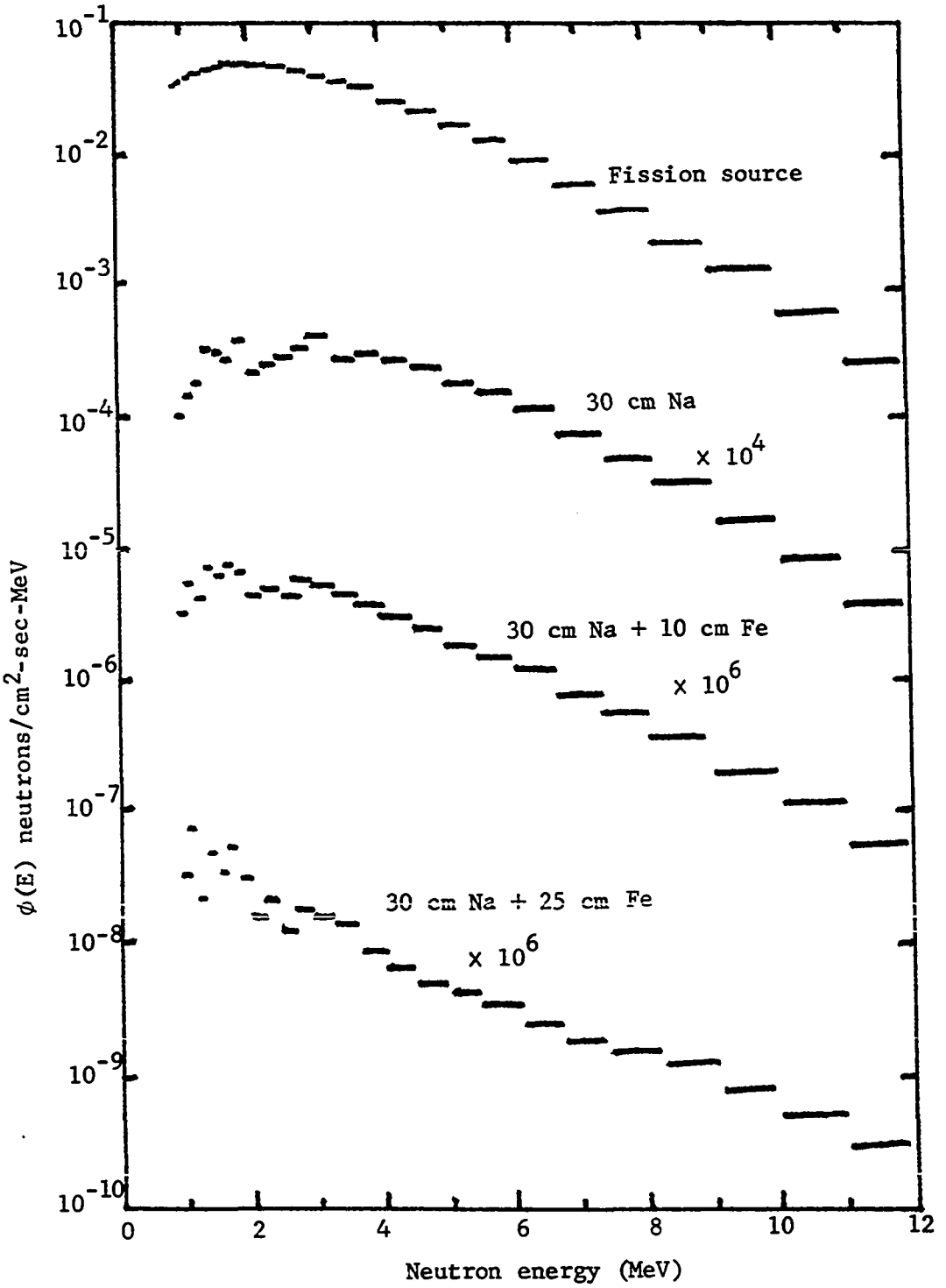


Fig. 21. Neutron spectra through sodium-iron multi-layers from a point isotropic fission source

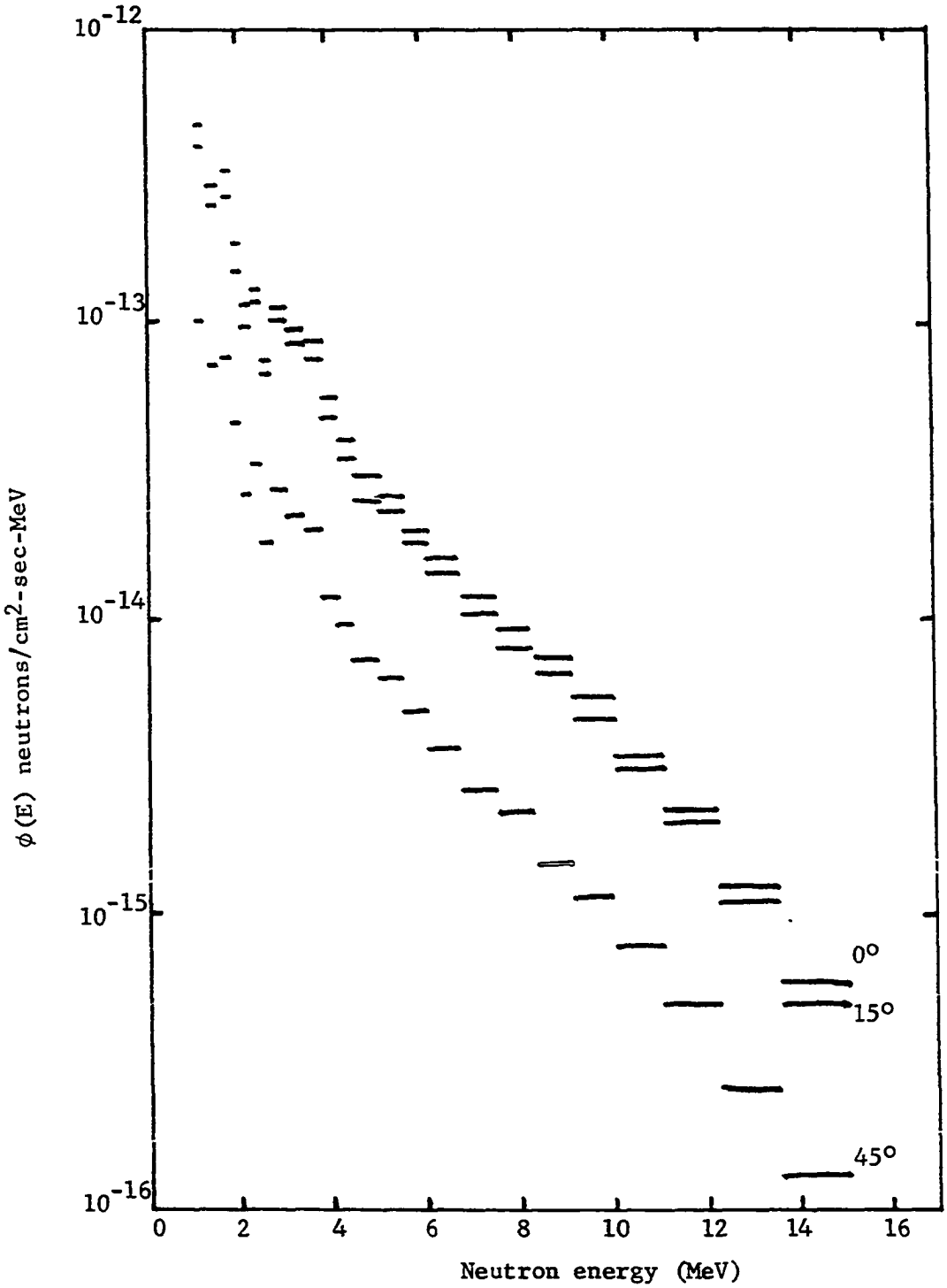


Fig. 22. Neutron spectra through 30 cm sodium and 25 cm iron layers at various angles from a point isotropic fission source

# VI. CONCLUSIONS

Within the scope of this investigation the following conclusions have been made.

(1) The modified transfer matrix, which is formulated to accept average group cross section data, is applicable for neutron shielding calculations. The results of this method depend upon the angular terms and energy groupings used in the calculation. The $P_2$ expansion underestimated the result and the $P_3$ expansion overestimated the result. However, a $P_6$ expansion should give satisfactory results, even if the fine energy grouping is used in the calculation.

(2) The essential computational advantage was retained by the modified transfer matrix method. The bulk of the computing time for a single problem goes into evaluating the eigenvalue spectrum and the eigendistributions. These are specific for each material but do not depend on the source geometry and shielding configurations.

(3) The developed higher order moments of the point matrix kernel gave good accomplishments in calculating transmitted and reflected angular distributions due to a point isotropic source. A good representation of the angular distributions can be obtained by taking higher order moments into account.

(4) The average total cross section of the iron in the region 1 to 2.5 MeV is shown to be high in the DLC-2/100G evaluations. For energies above 3 MeV, the average group cross sections

of the iron and sodium in the DLC-2/100G evaluations show good agreement with the experimental result.

# VII. SUGGESTIONS FOR FURTHER STUDY

As has been indicated previously the major problem in the investigation has been with the order of the double-$P_n$ expansion of the angular variable. Better accuracy can be obtained by using higher order polynomial. However, a higher order polynomial would increase the size of the problem considerably. As an alternative, angular dependence expanded in other polynomials could be tried.

With the fast neutron distribution obtained by the modified transfer matrix method, one could then calculate the secondary gamma sources due to inelastic scattering of fast neutrons. Coupling this secondary gamma source with that one due to thermal neutron capture, would yield a good approximation to the production and transmission of secondary gammas in a slab. Since the thermal neutron distribution is dependent upon the fast neutron distribution, the modified transfer matrix method could serve to obtain the thermal distribution as well.

A final suggestion for further investigation is the possibility of applying the higher order moments of the point matrix kernel to determine the angular flux distributions due to isotropic line, disk, and volume sources.

## VIII. BIBLIOGRAPHY


1. R. Aronson, Nuc. Sci. Eng., 51, 157 (1973).

2. R. Aronson, J. Math. Phys., 11, 931 (1970).

3. R. Aronson and D. L. Yarmush, J. Math. Phys., 7, 221 (1966).

4. R. E. Bellman, R. E. Kalaba, and G. H. Wing, J. Math. Phys., 1, 280 (1960).

5. B. G. Carlson, "Solution of the Transport Equation by $S_n$ Approximation," LA-1599, Los Alamos Scientific Lab. (1953).

6. G. Caroll and R. Aronson, Nuc. Sci. Eng., 51, 166 (1973).

7. K. M. Case and P. F. Zweifel, "Linear Transport Theory," Addison-Wesley, Reading, Massachusetts, 1967, Chapter 4.

8. M. Clark and K. F. Hansen, "Numerical Methods of Reactor Analysis," Academic Press, New York, 1964, Chapter 5.

9. V. A. Dulin, V. G. Dvukhsherstnov, Yu. A. Kazanskii, and I. V. Shugar, Soviet Atomic Energy, translated from Atomnaya Energiya, 17, 1249 (1964).

10. W. L. Filippone, Nuc. Sci. Eng., 52, 23 (1973).

11. S. Glasstone and A. Sesonske, "Nuclear Reactor Engineering," Van Nostrand Reinhold, New York, 1967, Chapter 10.

12. H. Goldstein and J. E. Wilkins, "Calculation of the Penetration of Gamma Rays," NYO-3075, Nuclear Development Associates (1954).

13. G. D. Joanon and J. S. Dudek, "GAM-II: A $B_3$ Code for the Calculation of Fast-Neutron Spectra and Associated Multigroup Constants," GA-4265, Gulf General Atomic (1963).

14. I. Kataoka, presented in Proceedings of the Third International Conference on the Peaceful Uses of Atomic Energy, Vol. 4, United Nations, New York, 1965.

15. Yu. A. Kazanskii, V. I. Kukhtevich, E. S. Matusevich, B. I. Sinitsyn, and S. G. Tsypin, "Physics of Reactor Shielding," S. G. Tsypin, Ed., Translated from Russian, Israel Program for Scientific Translations, Jerusalem, 1969, Chapter 8.

16. K. D. Lathrop, "DTF-IV, a FORTRAN-IV Program for Solving the Multigroup Transport Equation with Anisotropic Scattering," LA-3373, Los Alamos Scientific Lab. (1965).

17. L. Lois and J. Certaine, "A Round-off Free Solution of the Boltzmann Transport Equation in Slab Geometry," Advances in Nuclear Science and Technology, Vol. 5, E. J. Henley and J. Lewins, Ed., Academic Press, New York, 1969, pp. 325-368.

18. R. E. Maerker and F. J. Muckenthaler, Nuc. Sci. Eng., 52, 227 (1973).

19. D. R. Mathews, K. F. Hansen, and E. A. Mason, Nuc. Sci. Eng., 27, 263 (1967).

20. A. H. Maute, "Direct Determination of Transmission and Reflection Matrix for Gamma Rays," ORNL-Tr-2214, Oak Ridge Nat. Lab. (1968).

21. F. R. Mynatt, M. L. Gritzner, R. E. Maerker, and B. J. McGregor, "Fast Reactor Shielding Monthly Progress Report for January 1972," ORNL-TM-3746, Oak Ridge Nat. Lab. (1972).

22. G. H. Peebles and M. S. Plesset, Phys. Rev., 81, 430 (1951).

23. S. Preiser, G. Rabinowitz, and E. D. Dufour, "A Program for the Numerical Integration of the Boltzmann Equation-NIOBE," ARL Technical Report 60-314, Aeronautical Research Lab. (1960).

24. A. F. Rohach, "Application of the Transmission Matrix to Radiation Shielding," Final Report (ISU-ERI-AMES-72014), Engineering Research Institute, Iowa State University, Ames, Iowa (1972).

25. N. M. Schaeffer, "Reactor Shielding for Nuclear Engineers," TID-25951, USAEC Technical Information Center, Oak Ridge, Tennessee (1973).

26. K. Shure, Nuc. Sci. Eng., 19, 310 (1964).

27. A. W. Thiele, "Neutron and Gamma Attenuation in Sodium," NAA-SR-MEMO-12467, Atomics International (1967).

28. A. Weinberg and E. Wigner, "The Physical Theory of Neutron Chain Reactors," Chicago Univ. Press, Chicago, Illinois, 1958, Chapter 9.

29. D. L. Yarmush, J. Zell, and R. Aronson, "The Transmission Matrix Method for Penetration Problem," Technical Report 59-772, Wright Air Development Center (1960).

# IX. ACKNOWLEDGMENTS

The author wishes to express his gratitude to Dr. A. F. Rohach for his suggestions, guidance, and assistance in this investigation. Also, financial support by the Engineering Research Institute, Iowa State University, is gratefully acknowledged.

The author wishes to thank Drs. Glenn Murphy, R. A. Danofsky, G. H. Junkhan, and R. J. Lambert who, along with Dr. Rohach, formed his graduate committee.

It is also a pleasure to express appreciation to the Radiation Shielding Information Center, Oak Ridge National Laboratory, for supplying the neutron cross section data for use in this work.

Finally the author wishes to express his gratitude to his wife, Yuen-Ching, for her encouragement and understanding throughout his graduate study.

# X. APPENDIX

In this appendix is described the computations for

$$e_{mn} = \int_0^1 \omega P_n^+(\omega) P_m^+(\omega) d\omega \tag{17}$$

and

$$d_{mn}^{\ell}(\mu_o) = \int_0^1 d\omega P_\ell(\omega) P_m^+(\omega) \int_0^1 d\omega' P_\ell(\omega') P_n^+(\omega'). \tag{18}$$

The half-range Legendre polynomials obey the recurrence relation [8]

$$2(2n+1)\omega P_n^+(\omega) = (n+1)P_{n+1}^+(\omega) + (2n+1)P_n^+(\omega) + nP_{n-1}^+(\omega). \tag{A-1}$$

Substitution of Eq. (A-1) into Eq. (17), results in

$$\begin{aligned} e_{mn} &= \frac{n+1}{2(2n+1)} \int_0^1 P_{n+1}^+(\omega) P_m^+(\omega) d\omega + \frac{2n+1}{2(2n+1)} \int_0^1 P_n^+(\omega) P_m^+(\omega) d\omega \\ &\quad + \frac{n}{2(2n+1)} \int_0^1 P_{n-1}^+(\omega) P_m^+(\omega) d\omega \\ &= \frac{n+1}{2(2n+1)(2m+1)} \delta_{m,n+1} + \frac{1}{2(2m+1)} \delta_{m,n} \\ &\quad + \frac{n}{2(2n+1)(2m+1)} \delta_{m,n-1} . \end{aligned} \tag{A-2}$$

The orthogonality of the half-range Legendre polynomials was employed in Eq. (A-2). Based on Eq. (A-2), a $7 \times 7$ matrix E is shown in Table 4.

The evaluation of $d_{mn}^{\ell}(\mu_o)$ is done by the following method [17]. Define

$$f_{\ell m} = \int_0^1 P_\ell(\omega) P_m^+(\omega) d\omega. \tag{A-3}$$

Equation (18) becomes

Table 4. The matrix E ($e_{mn}$)

| n | m 0 | 1 | 2 | 3 | 4 | 5 | 6 |
|---|---|---|---|---|---|---|---|
| 0 | 1/2 | 1/6 | 0 | 0 | 0 | 0 | 0 |
| 1 | 1/6 | 1/6 | 1/15 | 0 | 0 | 0 | 0 |
| 2 | 0 | 1/15 | 1/10 | 3/70 | 0 | 0 | 0 |
| 3 | 0 | 0 | 3/70 | 1/14 | 2/63 | 0 | 0 |
| 4 | 0 | 0 | 0 | 2/63 | 1/18 | 5/198 | 0 |
| 5 | 0 | 0 | 0 | 0 | 5/198 | 1/22 | 3/143 |
| 6 | 0 | 0 | 0 | 0 | 0 | 3/143 | 1/26 |

$$d_{mn}^{\ell}(\mu_o) = f_{\ell m} f_{\ell n} \ . \qquad \text{(A-4)}$$

The relation between the full-range and half-range Legendre polynomials is

$$\bar{P}_m^+(\omega) = P_m(2\omega - 1).$$

Using the expansion for $P_m(2\omega - 1)$,

$$P_m(2\omega - 1) = \frac{2m - 1}{m} (2\omega - 1)P_{m-1}(2\omega - 1) - \frac{m - 1}{m} P_{m-2}(2\omega - 1),$$

Eq. (A-3) becomes

$$f_{\ell m} = \frac{2m - 1}{m} \int_0^1 2\omega P_\ell(\omega) P_{m-1}(2\omega - 1) d\omega - \frac{2m - 1}{m} \int_0^1 P_\ell(\omega) P_{m-1}(2\omega - 1) d\omega$$
$$- \frac{m - 1}{m} \int_0^1 P_\ell(\omega) P_{m-2}(2\omega - 1) d\omega.$$

Substituting

$$\omega P_\ell(\omega) = \frac{\ell}{2\ell+1} P_{\ell-1}(\omega) + \frac{\ell+1}{2\ell+1} P_{\ell+1}(\omega)$$

in the first term, and using the definition of $f_{\ell m}$, one obtains

$$f_{\ell m} = \frac{2m-1}{m} \frac{2\ell}{2\ell+1} f_{\ell-1,m-1} + \frac{2m-1}{m} \frac{2(\ell+1)}{2\ell+1} f_{\ell+1,m-1}$$

$$- \frac{2m-1}{m} f_{\ell,m-1} - \frac{m-1}{m} f_{\ell,m-2} \cdot \qquad \text{(A-5)}$$

This recursion relation suggests that the calculation of $f_{\ell m}$ can be achieved if $f_{\ell,m-2}$, $f_{\ell-1,m-1}$, $f_{\ell,m-1}$, and $f_{\ell+1,m-1}$ are known. To start off a calculation like this, the first and second columns must be known as well as the first row.

The first column can be computed as follows:

$$f_{\ell,0} = \int_0^1 P_\ell(\omega) d\omega.$$

By means of the relation

$$\int_0^1 P_\ell(\omega) d\omega = \frac{-\ell+2}{\ell+1} \int_0^1 P_{\ell-2}(\omega) d\omega = \frac{-\ell+2}{\ell+1} f_{\ell-2,0} , \qquad \text{(A-6)}$$

and using $f_{0,0} = 1$ and $f_{2,0} = 0$, it is obvious that all the even numbers of the first column are equal zero.

But $f_{1,0} = 1/2$; therefore, one obtains $f_{3,0} = -1/8$, $f_{5,0} = 1/16$, $f_{7,0} = -5/128$, etc. The second column can be computed similarly

$$f_{\ell,1} = \int_0^1 P_\ell(\omega)(2\omega - 1) d\omega$$

$$= \frac{2\ell}{2\ell+1} \int_0^1 P_{\ell-1}(\omega) d\omega + \frac{2(\ell+1)}{2\ell+1} \int_0^1 P_{\ell+1}(\omega) d\omega - \int_0^1 P_\ell(\omega) d\omega$$

$$= \frac{2\ell}{2\ell+1} f_{\ell-1,0} + \frac{2(\ell+1)}{2\ell+1} f_{\ell+1,0} - f_{\ell,0} \cdot \qquad \text{(A-7)}$$

Finally one notes that $f_{\ell m} = 0$ for $m > \ell$. To prove this, expand $P_\ell(\omega)$:

$$P_\ell(\omega) = \sum_{k=0}^{\ell} A'_k P_k(2\omega - 1),$$

$$f_{\ell m} = \sum_{k=0}^{\ell} A'_k \int_0^1 P_k(2\omega - 1) P_m(2\omega - 1) d\omega$$

$$= \sum_{k=0}^{\ell} \frac{1}{2} A'_k \int_{-1}^{1} P_k(x) P_m(x) dx.$$

For $m > \ell$, $f_{\ell m} = 0$, therefore $f_{\ell m}$ is a low triangular matrix.

By means of Eqs. (A-5), (A-6), and (A-7), $f_{\ell m}$ can be calculated to the desired size. Similarly, $f_{\ell n}$ in Eq. (A-4) can be obtained in the same way.

Before substituting $f_{\ell m}$ and $f_{\ell n}$ into Eq. (A-4), the symmetric property $d^{\ell}_{mn}(\mu_o)$ is noted. By virtue of the Legendre property $P_\ell(-\omega) = (-1)^\ell P_\ell(\omega)$, $d^{\ell}_{mn}(\mu'_o)$ can be calculated as follows:

$$d^{\ell}_{mn}(\mu'_o) = \int_0^1 d\omega P_\ell(\omega) P^+_m(\omega) \int_0^1 d\omega' P_\ell(-\omega') P^+_n(\omega')$$

$$= (-1)^\ell f_{\ell m} f_{\ell n}$$

$$= (-1)^\ell d^{\ell}_{mn}(\mu_o). \qquad \text{(A-8)}$$

In Table 5 is given the elements of $f_{\ell m}$ for $\ell = 6$.

Table 5. The elements of $f_{\ell m}$

| $\ell$ | m | | | | | | |
|---|---|---|---|---|---|---|---|
| | 0 | 1 | 2 | 3 | 4 | 5 | 6 |
| 0 | 1 | 0 | 0 | 0 | 0 | 0 | 0 |
| 1 | 1/2 | 1/6 | 0 | 0 | 0 | 0 | 0 |
| 2 | 0 | 1/4 | 1/20 | 0 | 0 | 0 | 0 |
| 3 | -1/8 | 1/8 | 1/8 | 1/56 | 0 | 0 | 0 |
| 4 | 0 | -1/24 | 1/8 | 1/16 | 1/144 | 0 | 0 |
| 5 | 1/16 | -1/16 | 1/32 | 3/32 | 1/32 | 1/352 | 0 |
| 6 | 0 | 1/64 | -3/64 | 1/16 | 1/16 | 1/64 | 1/832 |